DIPLOMARBEIT

Satellite Scheduling with VieSched++

zur Erlangung des akademischen Grades

Diplom-Ingenieur

ausgeführt am Department für

Geodäsie und Geoinformation

Forschungsbereich Höhere Geodäsie

der Technischen Universität Wien

unter Anleitung von

Univ.Prof. Dipl.-Ing. Dr.techn. Johannes Böhm

und

Dipl.-Ing. Dr.techn. Matthias Schartner

durch

Helene Wolf BSc

Matrikelnummer: 01426131

Wien, im Februar 2021

Unterschrift (Verfasser/in)

Unterschrift (Betreuer/in)

Eidesstaatliche Erklärung

Ich erkläre an Eides statt, dass die vorliegende Arbeit nach den anerkannten Grundsätzen für wissenschaftliche Abhandlungen von mir selbstständig erstellt wurde. Alle verwendeten Hilfsmittel, insbesondere die zugrunde gelegte Literatur, sind in dieser Arbeit genannt und aufgelistet. Die aus den Quellen wörtlich entnommenen Stellen, sind als solche kenntlich gemacht.

Das Thema dieser Arbeit wurde von mir bisher weder im In- noch Ausland einer Beurteilerin/einem Beurteiler zur Begutachtung in irgendeiner Form als Prüfungsarbeit vorgelegt. Diese Arbeit stimmt mit der von den Begutachterinnen/Begutachtern beurteilten Arbeit überein.

Wien, im Februar 2021 _____

Acknowledgements

First of all, I would like to sincerely thank Prof. Johannes Böhm for his continuous support from the beginning. He always found a moment to help me with my concerns and his guidance helped me to overcome all difficulties. I am very grateful to have had the chance to work in his research group.

I also want to express my deep gratitude to Matthias Schartner for supervising me in all kind of aspects since I joined the VLBI group. Thanks for always supporting me no matter which problem occurred.

Another thank goes to my former and present colleagues at the higher geodesy group at TU Wien for the friendly working atmosphere, support and helpful attitude.

Moreover, I would like to thank all my friends for always being there for me. I am also happy that many of my study colleagues became good friends who accompanied me during the years. Thanks for all the fun, support and experiences we gained together.

Finally, I would like to express my gratitude to my family who have always been there for me and constantly support me in every situation of life. Without the major backing of my family I would not be where I am now.

Kurzfassung

Very Long Baseline Interferometry (VLBI) ist ein geodätisches Weltraumverfahren, welches mit global verteilten Teleskopen extragalaktische Radioquellen beobachtet. In den letzten Jahren wurden Ideen vorgeschlagen, einen oder mehrere Satelliten der zweiten Generation des Galileo-Satellitensystems mit einem VLBI Transmitter auszustatten. Beobachtungen zu Satelliten mit VLBI Teleskopen stellen eine Vielzahl an neuen Möglichkeiten, wie die direkte Bestimmung der absoluten Orientierung des Satellitenorbits in Bezug auf den internationalen himmelsfesten Referenzrahmen (ICRF, International Celestial Reference Frame) und eine Verbesserung der Verknüpfung der Referenzrahmen der verschiedenen geodätischen Weltraumverfahren, dar.

Da mehrere Teleskope eine Quelle gleichzeitig beobachten müssen, ist es notwendig einen Beobachtungsplan zu erstellen. Herkömmliche, zur Erstellung von Beobachtungsplänen verwendete, Softwarepakete unterstützen die Planung von Beobachtungen zu Quasaren aber nur wenige die Planung von Beobachtungen zu Satelliten. Die neu entwickelte Software VieSched++ wurde mit einem Modul ausgestattet, welches es ermöglicht Beobachtungspläne mit Beobachtungen zu Quasaren und Satelliten zu erzeugen. In dieser Arbeit wird ein Überblick über dieses neue Modul gegeben und die verschiedenen Methoden um Satellitenbeobachtungen in Beobachtungspläne zu integrieren, beschrieben.

Weiters behandelt diese Arbeit eine Evaluierungsstudie von möglichen Beobachtungen zu Galileo-Satelliten mit einem VLBI Netzwerk. Die möglichen Zeiträume, während deren ein Satellit beobachtet werden kann, werden mit Hilfe des neuen Moduls in VieSched++ bestimmt. Diese möglichen Beobachtungen werden hinsichtlich der Sichtbarkeit, die Anzahl der Stationen von denen ein Satellit beobachtet werden kann, und dem Einfluss der Beobachtungsgeometrie zwischen der beobachtenden Stationen und der Position des Satelliten auf die direkte Bestimmung der absoluten Orientierung des Satellitenorbits in Bezug auf den ICRF bewertet.

Die Studie zeigt, dass die Galileo-Satelliten eine hohe Sichtbarkeit für ein VLBI Netzwerk aufweisen. Es gibt keine Unterschiede hinsichtlich der Sichtbarkeit der einzelnen Bahnen der Galileo Konstellation und der einzelnen Positionen der Satelliten innerhalb einer Bahn. Falls ein Satellit mit einem VLBI Transmitter ausgestattet wird, gibt es daher keine zu bevorzugende Bahn oder Position innerhalb einer Bahn für die Platzierung des Satelliten. Die Untersuchung der besten Konfiguration zweier mit einem VLBI Transmitter ausgestatteten Satelliten zeigt, dass es Unterschiede gibt, ob die Satelliten innerhalb derselben Bahn oder in unterschiedlichen Bahnen sind.

Abstract

Very Long Baseline Interferometry (VLBI) is a space-geodetic technique observing extragalactic radio sources with globally distributed radio telescopes. Over the last years, ideas have been proposed to equip one or more satellites of the second generation of the Galileo constellation with a VLBI transmitter. Observations of satellites with VLBI antennas provide a variety of new possibilities such as the direct determination of the absolute orientation of the satellite orbit with respect to the International Celestial Reference Frame (ICRF) and providing space ties instead of using local ties for connecting reference frames of different space-geodetic techniques.

As more VLBI antennas have to observe a source simultaneously, it is necessary to create an observation plan, a so-called schedule. Common scheduling software packages support the scheduling of observations to extragalactic radio sources but only a few are able to schedule observations to satellites. The newly developed scheduling software VieSched++, written in C++, was equipped with a satellite scheduling module which allows the generation of a schedule including both, observations to quasars and satellites. In this work, an overview about the new satellite scheduling module in VieSched++ is given and the different available approaches to schedule satellite observations, the semi-manual and the automatic approach, are described.

Moreover, this thesis deals with an evaluation study of possible satellite observations to Galileo satellites from a VLBI network. The time periods during which a satellite is observable from the VLBI network are determined using the satellite scheduling module in VieSched++. The possible satellite observations are evaluated through the number of stations from which the satellite could be observed and by the impact on determining the orientation of the satellite constellation directly with respect to ICRF, caused by the observation geometry.

The study shows that Galileo satellites exhibit a high visibility for a VLBI network. There are no differences in terms of visibility between the individual orbital planes of the Galileo constellation and between the different orbital positions within these planes. If one satellite would be equipped with a VLBI transmitter there is therefore no preferable plane or slot within a plane to place this satellite. The investigation of the best combination of two satellites equipped with a VLBI transmitter shows that it has to be distinguished if the satellites are within the same plane or in different orbital planes.

Contents

Kurzfassung IV

Abstract VI

List of Figures X

List of Abbreviations XII

1. Introduction 1

1.1. Objectives of this thesis . . . 1

1.2. Thesis structure . . . 2

2. Very Long Baseline Interferometry and Galileo satellite system 3

2.1. Very Long Baseline Interferometry . . . 3

2.1.1. Geometric principle of VLBI . . . 4

2.1.2. Scheduling . . . 5

2.1.3. Correlation . . . 6

2.1.4. Simulation . . . 6

2.1.5. Analysis . . . 7

2.1.6. Products . . . 8

2.1.7. VGOS . . . 8

2.2. Galileo satellite system . . . 9

2.2.1. Orbital elements . . . 9

2.2.2. System description . . . 11

3. Satellite observations with VLBI 15

3.1. Applications . . . 15

3.1.1. Determination of absolute orientation of satellite constellation . . . 15

3.1.2. Terrestrial Reference Frame . . . 15

3.2. Scheduling of Satellite Observations . . . 18

3.2.1. Visibility . . . 19

3.2.2. Antenna slew rates . . . 21

3.2.3. Sun distance . . . 23

3.2.4. Cable wrap . . . 24

3.3. Satellite Orbit Prediction . . . 25

3.3.1. Accuracy of Orbits . . . 25

3.3.2. Data Formats . . . 25

3.3.3. Orbit propagation with TLE Data 26

4. Method **29**

4.1. Visibility of a satellite 29
4.1.1. Satellite position as ECI coordinates 29
4.1.2. Station position as ECI coordinates 30
4.1.3. View angles 30
4.2. Satellite Scheduling with VieSched++ 32
4.2.1. Input data 33
4.2.2. Semi-manual Mode 33
4.2.3. Automatic Mode 38

5. Evaluation study of satellite observations **39**

5.1. VLBI network 39
5.2. Galileo satellites 40
5.3. Evaluation through visibility 41
5.3.1. Visibility in percent 41
5.3.2. Visibility over session time 44
5.3.3. Visibility of satellite trajectories 46
5.3.4. Visibility over repeat period of Galileo 49
5.4. Evaluation through observation geometry 53
5.4.1. Estimation of RAAN from VLBI observations 53
5.4.2. UT1-UTC Dilution of Precision factor 53
5.4.3. Results and analysis of UDOP factor 55
5.5. Discussion of results 59
5.5.1. One satellite equipped with VLBI transmitter 59
5.5.2. Two satellites equipped with VLBI transmitter 59

6. Summary and Conclusion **69**

A. Coordinate systems **73**

A.1. Earth-Centered Inertial System 73
A.2. Topocentric Horizon Coordinate System 75

References **77**

List of Figures

2.1. Geometric measurement principle of VLBI 4
2.2. Keplerian elements 10
2.3. Galileo constellation 12
2.4. Configuration of the Galileo constellation 13
3.1. Concept of local ties and space ties 18
3.2. Geometry of satellite observations with VLBI antennas 19
3.3. Horizon mask 20
3.4. Keyholes for different VLBI antenna mount types 23
3.5. Antenna cable wrap 24
4.1. Topocentric Horizon Coordinate System 31
4.2. Ground track 34
4.3. Elevation angles over time 34
4.4. Percentage of visibility from a certain number of stations 35
4.5. Percentage of visibility stacked for whole session 35
4.6. Determination of possible scans 36
4.7. Elevation angles over time of possible scan 37
4.8. Skyplot of possible scan 37
5.1. VLBI Network 39
5.2. Visibility in percent - Plane A 42
5.3. Visibility in percent - Plane B 42
5.4. Visibility in percent - Plane C 43
5.5. Visibility over session time - Plane A 44
5.6. Visibility over session time - Plane B 45
5.7. Visibility over session time - Plane C 45
5.8. Ground track of GSAT0205 (E24) 47
5.9. Ground track of GSAT0216 (E25) 47
5.10. Ground track of GSAT0215 (E21) 48
5.11. Ground track of GSAT0217 (E27) 48
5.12. Visibility over repeat period of Galileo - Plane A 50
5.13. Visibility over repeat period of Galileo - Plane B 51
5.14. Visibility over repeat period of Galileo - Plane C 52
5.15. UDOP values of GSAT0102 (E12) 57
5.16. UDOP values of GSAT0101 (E11) 58

5.17. Visibility over time of two satellites in Plane A in consecutively slots . . 61
5.18. Visibility over time of two satellites in Plane A in slots widest apart . . . 61
5.19. Ground tracks of two satellites within Plane A 62
5.20. Ground tracks of one satellite per Plane A and one per Plane B 65
5.21. Ground tracks of one satellite per Plane B and one per Plane C 66
5.22. Ground tracks of one satellite per Plane C and one per Plane A 67
A.1. Earth-Centered Inertial System 74
A.2. Topocentric Horizon Coordinate System 75

List of Abbreviations

AzEl Azimuth-Elevation antenna mount

CPF Consolidated Prediciton Format

CRF Celestial Reference Frame

DOP Dilution of Precision

DORIS Doppler Orbitography and Radiopositioning Integrated by Satellite

ECI Earth-centered inertial

EOP Earth Orientation Parameters

ESA European Space Agency

GGOS Global Geodetic Observing System

GNSS Global Navigation Satellite Systems

GUI Graphical User Interface

HaDec Equatorial antenna mount

ICRF International Celestial Reference Frame

IERS International Earth Rotation and Reference Systems Service

IGS International GNSS Service

ILRS International Laser Ranging Service

ITRF International Terrestrial Reference Frame

IVS International VLBI Service for Geodesy and Astrometry

LSM Least Squares Method

MEO Medium Earth Orbit

NORAD North American Aerospace Defence Command

RAAN Right Ascension of the Ascending Node

SDP Simplified Deep Space Perturbation

SGP Simplified General Perturbation

SLR Satellite Laser Ranging

SNR Signal to Noise Ratio

SP3 Standard Product 3

TLE Two-Line Element

TRF Terrestrial Reference Frame

UDOP UT1-UTC Dilution of Precision

UT1 Universal Time

UTC Coordinated Universal Time

VGOS VLBI Global Observing System

VieVS Vienna VLBI and Satellite Software

VLBI Very Long Baseline Interferometry

ccw counter-clockwise cable wrap

cw clockwise cable wrap

n neutral cable wrap

1. Introduction

Very Long Baseline Interferometry (VLBI) forms together with Global Navigation Satellite Systems (GNSS), Satellite Laser Ranging (SLR), and Doppler Orbitography and Radiopositioning Integrated by Satellite (DORIS) the four space-geodetic techniques. Geodetic VLBI measures the difference in arrival times of microwave signals emitted from extragalactic radio sources at two or more VLBI stations.

As VLBI is observing very stable extragalactic radio sources, it is able to determine the International Celestial Reference Frame (ICRF) and relate the positions of the telescopes on Earth to the stable celestial background. Therefore, VLBI is the only technique which is able to determine the absolute orientation of the Earth in space representing a benefit over the other space-geodetic techniques.

Over the last years, ideas have been proposed to equip one or more satellites of the second generation of the Galileo constellation with a VLBI transmitter. This provides the opportunity of extending the current VLBI research with observations to satellites and offers a variety of new possibilities such as the direct determination of the absolute orientation of a satellite orbit with respect to the ICRF. Further, interesting scientific applications can be found in providing space ties instead of local ties for connecting reference frames of different space-geodetic techniques.

1.1. Objectives of this thesis

In this thesis the new possibility for including observations to satellites in a schedule using the VLBI scheduling software VieSched++ is presented. VieSched++ has been recently developed at TU Wien. The software is written in C++ and has a modern Graphical User Interface (GUI) which makes it easy to use. A satellite scheduling module was successfully implemented in the software which allows the scheduling of observations to satellites. There are two approaches available to schedule satellite observations, the semi-manual and the automatic mode. The procedures of the two different approaches and the interaction of the scheduler are described.

Further, this thesis includes an evaluation study of satellite observations to Galileo satellites from a VLBI network. The possible observations are determined using the newly developed satellite scheduling module in VieSched++. The possible satellite observations are evaluated through the number of stations from which the satellite is visible and by the observation geometry between the observed baselines and the position of the satellite using the UT1-UTC Dilution of Precision (UDOP) factor.

1.2. Thesis structure

First, an introduction to geodetic VLBI and the Galileo satellite system is given in section 2. This is followed by a detailed insight in the field of satellite observations with VLBI antennas in section 3, including the applications these observations provide, the requirements of scheduling observations to satellites and the aspects of predicting satellite orbits. Section 4 refers to the developed satellite scheduling module in VieSched++. The computation of possible observation periods is outlined followed by a comprehensive description of the two different approaches for scheduling satellite observations.

Section 5 is related to possible observations to Galileo satellites from a VLBI network. The visibility of the satellites is evaluated through the number of stations from which the satellites are observable and is investigated in different aspects such as the percentage of time the satellites are visible and the changes of the visibility over the session time and over the repeat period of Galileo. Further, the possible satellite observations are evaluated by the impact of the observation geometry between the observed baselines and the position of the satellite on the direct determination of the orientation of the satellite orbit with respect to ICRF.

Section 6 provides a summary and conclusion concerning the discussed and presented topics.

2. Very Long Baseline Interferometry and Galileo satellite system

This section provides an overview about VLBI and the Galileo satellite system. First, the geometrical principle of VLBI is outlined followed by an outline of the different aspects of planning and processing VLBI data including scheduling, correlation, simulation and analysis. Finally, the products of VLBI are described and a brief insight in the new VLBI Global Observing System (VGOS) is given.

Further, the Galileo satellite system is described as the European GNSS. A short overview about the orbital elements is given, followed by a description of the satellite constellation.

2.1. Very Long Baseline Interferometry

In standard geodetic VLBI extragalactic radio sources, called quasars, are observed by two or more radio telescopes simultaneously which are globally distributed over the Earth. This technique contributes to the determination of the Terrestrial Reference Frame (TRF) (Altamimi et al., 2016), especially in terms of its scale, and it is further essential for realizing the Celestial Reference Frame (CRF) (Charlot et al., 2020). Moreover, VLBI is used for the determination of the Earth's orientation in space which is important for positioning and navigation on the Earth's surface and in space.

VLBI is the only geodetic technique able to monitor the full set of Earth Orientation Parameters (EOP). This set of parameters consists of two angles for precession and nutation (dX, dY) which are describing the motion of the Earth's rotation axis in the celestial reference frame, two angles for polar motion (*xpol, ypol*) describing the motion of the Earth's rotation axis in the terrestrial reference frame and one angle describing the rotation of the Earth around its axis, the Earth rotation angle *dUT1* (Petit and Luzum, 2010). Especially the parameter *dUT1*, the difference between Universal Time (UT1) and Coordinated Universal Time (UTC) and the parameters of precession and nutation can be uniquely determined with VLBI (Schuh and Böhm, 2013).

VLBI requires cooperating observatories globally distributed over the Earth in order to carry out observations and obtain products. The VLBI observations are organized by the International VLBI Service for Geodesy and Astrometry (IVS) which is an international collaboration of organizations operating or supporting VLBI components (Nothnagel et al., 2017).

2.1.1. Geometric principle of VLBI

VLBI measures the difference in arrival time of microwave signals emitted from objects, mostly extragalactic radio sources. Thus, at least two VLBI telescopes have to observe the same source simultaneously. The received signals are marked with time stamps and recorded at all observing stations and further cross-correlated to derive the time difference in signal reception at the stations, the time delay τ. The geometric principle of VLBI is shown in Figure 2.1.

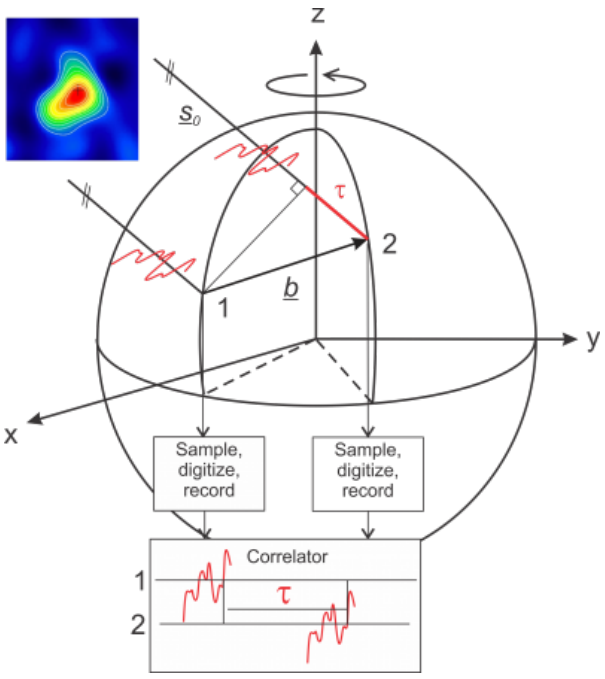

Figure 2.1: Geometric measurement principle of VLBI, from Schuh and Böhm (2013).

As a result of the long distance between the Earth and the extragalactic sources, which is up to billions of light years, the incoming radiation can be assumed to arrive in plane wavefronts on Earth and the direction to the source $\vec{s_0}$ becomes parallel for all ground-based stations. Therefore, the geometric principle of VLBI reduces to a right-angled triangle. The observed time difference in arrival times τ between the reception time at station 1 (t_1) and station 2 (t_2) can be expressed as the negative scalar product of the baseline vector $\vec{b}$ between the two stations and the direction to the quasar $\vec{s_0}$ scaled by the speed of light c, see equation 2.1 (Schuh and Böhm, 2013).

$$\tau = -\frac{\vec{b} \cdot \vec{s_0}}{c} = t_2 - t_1 \tag{2.1}$$

The antennas observe the radio sources in two frequency bands, the S-band (2.3 GHz) and the X-band (8.4 GHz), in order to correct for dispersive effects on the radio signal caused by the Ionosphere.

2.1.2. Scheduling

As described in the section 2.1.1, the VLBI technique requires observations to the same radio source with a net of at least two telescopes at the same time. Two stations observing the same source form a so-called baseline which represents an observation. If a net of n antennas observes the same radio source at the same time in total $n \cdot (n-1)/2$ baselines are observed. These simultaneous observations to the same source from two or more antennas form a so-called scan.

An observation plan, a so-called schedule, is necessary to coordinate the observations during the whole experiment between the radio telescopes which are globally distributed over the Earth. Scheduling is crucial for the feasibility of a session and influences the quality of the derived geodetic parameters. The generation of a schedule is a complex task and can be seen as an optimization process (Schartner and Böhm, 2019).

A schedule defines for each station which sources should be observed in which order and when the observation will start and stop (Schartner, 2019). The schedule contains a list of scans, ordered by time, for the whole VLBI experiment.

Creating a schedule is a complex task with many parameters and requirements taken into account. The visibility of a source from an antenna is, additionally to the fact that the source is above the horizon, dependent on the horizon mask of the specific antenna. The time of observing a source, the so-called on-source time, should be long enough to achieve a proper Signal to Noise Ratio (SNR) and is dependent on the antenna sensitivity but also on the flux density emitted by the observed source. The observation duration is calculated per baseline and therefore it can be different for each pair of antennas observing the same source. The time an antenna needs to slew from one source to the other source of two sequent scans is dependent on its slew rates. All these parameters, visibility, scan duration, slew rates and many more have to be considered to enable successful observations and have an influence on the quality of the derived geodetic products.

Due to the complexity of generating VLBI schedules it can be done using dedicated software packages like sked (Vandenberg, 1999), sched (Walker, 2018), Vie_Sched (Sun, 2013) and VieSched++ (Schartner and Böhm, 2019). Currently, the software sked which is developed and maintained by the Goddard Space Flight Center's IVS Analysis Center

(GSFC) is widely used in the VLBI community and in the past almost all geodetic sessions were scheduled with this software. The package sched is developed at the National Radio Astronomy Observatory (NRAO) and is mostly used for astronomical applications. Vie_Sched is a module of the Vienna VLBI and Satellite Software (VieVS; (Böhm et al., 2018)) and was in the past used to schedule AUSTRAL sessions (Plank et al., 2017) with the AuScope geodetic VLBI array in Australia (Lovell et al., 2013).

The scheduling software VieSched++ has been recently developed at the TU Wien and is replacing the Vie_Sched module. Starting in 2018 several observing programs (AUA, T2, EURR&D, EUR, OHG, INT3,...) are now scheduled using this modern and new software VieSched++.

Each of these software packages supports the scheduling of observations to radio sources. In 2014 Vie_Sched was updated with features to enable the scheduling of observations to satellites along with observations to quasars (Hellerschmied et al., 2017). As VieSched++ is replacing the scheduling module Vie_Sched in VieVS a satellite scheduling module was implemented in VieSched++ as well. This newly developed module enables the scheduling of observations to satellites either in a semi-manual or in an automatic mode which is described in detail in section 4.

2.1.3. Correlation

The received signal is digitized and time-tagged using stable time signals provided by the station's atomic clock. Further, it is recorded on hard disks and sent to the correlation centers. At the correlator facility the signals from the antennas are combined pairwise in order to obtain the delay in signal reception times τ for each baseline by comparing the recorded bit streams. The signals of two antennas are shifted in time relatively to each other until the cross-correlation function is maximized (Nothnagel, 2019). Nowadays, software correlators, like the Distributed FX software correlator (DiFX; Deller et al., 2007 and Deller et al., 2011) are widely used.

2.1.4. Simulation

Carrying out VLBI experiments is associated with high costs and therefore it may be impractical to create VLBI data in order to validate and test new concepts, scheduling strategies or different station network geometries. The investigation of impacts of new concepts on the quality of VLBI products in an analytical fashion is difficult due to the complex interactions in VLBI analysis. Therefore, simulation studies are suitable for doing these investigations.

VLBI observations are simulated with a Monte-Carlo simulator which generates artificial observations by randomly simulating the error sources zenith wet delay (zwd_1 and zwd_2), the instability of the station clocks (clk_1 and clk_2) and white noise τ_{rnd} at the stations forming a baseline.

The simulated delay τ_{sim} consists of the geometric part τ_{g} and the three major errors sources, as it is expressed in equation 2.2.

$$\tau_{\mathrm{sim}} = \tau_{\mathrm{g}} + (zwd_2 \cdot mf(el_2) + clk_2) - (zwd_1 \cdot mf(el_1) + clk_1) + \tau_{\mathrm{rnd}} \tag{2.2}$$

The parameters el_1 and el_2 represent the elevation angle at the two stations observing the source. The fluctuations of water vapor and zenith wet delay can be simulated following an approach by Nilsson et al. (2007). The calculated zenith wet delay can be mapped with the wet mapping function mf to slant directions. The instability of the station clocks are modelled as the sum of the random walk and integrated random walk (Herring et al., 1990). The white noise τ_{rnd} can be modelled with the standard Gaussian white noise process.

2.1.5. Analysis

The final stage of the processing chain is the analysis of the VLBI data. The theoretical delay is modelled for each observation based on the a-priori information and by using models with high precision according to the International Earth Rotation and Reference Systems Service (IERS) conventions (Petit and Luzum, 2010). Some effects are too variable and hard to predict, like the tropospheric wet delay and the clock drifts, therefore these parameters have to be estimated as well and cannot be modelled. The difference between the observed and the modelled delay can be used to estimate various parameters of interest using methods like the Gauss-Markow Least Squares Method (LSM) or the Kalman filter. The LSM deals with the problem of deriving values of parameters of a mathematical model based on a set of observations. With a higher number of observations than necessary, it is possible to derive the values of the parameters in the model more accurate. This leads to the subject of solving an over-determined system of equations and the condition that minimizes the weighted sum of squared residuals. The least-square parameter estimation requires linear observation equations which is achieved by linearising the observation equation by a first-order Taylor polynom.

The parameters which can be estimated from a single session are for instance station coordinates, source coordinates, EOP, troposphere estimates and clock parameters.

The results of the individual VLBI sessions can be collected and analyzed together in a global solution by stacking the normal equation matrices. This makes it possible to combine the results of the whole history of VLBI sessions to estimate parameters with a high degree of accuracy and is commonly used for estimating a TRF or CRF, see (Krásná et al., 2014) and (Mayer, 2019).

2.1.6. Products

As already mentioned in section 2.1, VLBI is the only technique providing the full set of EOP and determining the CRF through positions of the extragalactic radio sources. Furthermore, it is important for realizing the TRF, especially in terms of its scale. Therefore, official IVS products are the maintenance of the TRF with station positions and their changes over time, the realization of the CRF and the generation of EOP time series.

VLBI observations can be also used to study interactions within the Earth's system. VLBI can determine geodynamic and atmospheric parameters such as Love numbers h and l of the solid Earth tides model (Spicakova et al., 2010), ionosphere models (Hobiger et al., 2006), or troposphere parameters.

2.1.7. VGOS

In the early 2000's the Global Geodetic Observing System (GGOS) (Plag and Pearlman, 2009) defined an ambitious goal of the realization of a TRF with 1-mm accuracy of station positions and 0.1-mm per year accuracy of station velocities.

In order to reach this, it is necessary to reduce the impact of error components. Simulation studies (Pany et al., 2010) showed that the impact of the troposphere, a dominant error source in VLBI, can be reduced by decreasing the source switching interval and therefore increasing the sampling of the sky. The total time, which is needed in order to observe a source, consists of the on-source time, the time which is needed to reach a certain SNR and the slew time between consecutive scans. To achieve short source-switching intervals both time periods have to be minimized.

The current VLBI system (S/X system, also called legacy system) consists of large and slow slewing antennas and makes it therefore difficult to achieve the target accuracy of GGOS. Therefore, changes are required in the field of VLBI and a next-generation VLBI system (conventionally called VLBI2010, but later renamed to VLBI Global Observing System (VGOS)) has been developed (Niell et al., 2005).

The new VGOS-type stations have a different telescope structure and a redesigned VLBI signal chain. The antennas are designed to have small dishes, around 12 meters, and higher slew rates to allow a fast switching between the sources. In order to compensate the loss of sensitivity due to the smaller dish and to reduce the on-source time, the frequency setup changed from two fixed bands, the S- and the X-band, to four or more observing bands in the range from 2 GHz to 14 GHz. Nowadays, VGOS observations are recorded with high data rates of 8 Gbit/s at four frequency bands.

The VGOS antennas are also more suitable for the tracking of satellites due to the small and fast antennas compared to the legacy antennas, which are mostly large and slow. Further, the new receiver system allows to observe satellite signals in a larger frequency range and is not restricted to the S- and X-band.

Due to the smaller antenna dish the antenna has a wider beamwidth as this is dependent on the antenna diameter D and on the wavelength of the observed radio signal λ. The width of the main lobe is commonly considered with the Half Power Beam Width (HPBW) which is defined as the angular separation at which the magnitude of the radiation pattern decreases by 50% from the peak of the main beam and can be approximated according to equation 2.3. With a wider antenna beam width, it is easier to keep the satellite accurately within the field view.

$$HPBW \sim \frac{\lambda}{D} \tag{2.3}$$

2.2. Galileo satellite system

Galileo is the GNSS of Europe and went in operation in 2016. It, as the other GNSS, refers to a constellation of satellites that provide signal broadcasts including the information of position and time the message was sent to GNSS receivers. This information is used by the receivers to determine their location on the Earth's surface. It was created by the European Union through the European Space Agency (ESA) and is operated by the European GNSS Agency (GSA). It will in total consist of 24 active satellites, which will be expected by 2021.

2.2.1. Orbital elements

A satellite orbits around the Earth in a plane. The orbit of a satellite can be defined with a set of numerical values called orbital or Keplerian elements. These elements consist of six parameters, illustrated in Figure 2.2 and described in the following.

- a - *semi-major axis of the orbital ellipse*, specifies the semi-major axis of the ellipse.
- e - *numerical eccentricity of the orbit* defines the eccentricity of the orbital plane. The eccentricity describes how much the ellipse deviates from a circle.
- i - *inclination of orbital plane* is the vertical tilt of the ellipse, the angle between the equatorial plane and the orbital plane.
- Ω - *right ascension of the ascending node* represents the angle between the direction of the ascending node and the vernal equinox, which is the intersection point between the Sun's trajectory and the equatorial plane of the Earth.
- ω - *argument of perigee* represents the angle between the direction of the ascending node and the direction of the perigee, measured along the orbital plane. The perigee is defined as the point in the orbital plane which is closest to the Earth's center of mass.
- v - *true anomaly at epoch* t_0 defines the position of the satellite in the orbit at a specific time t_0. It represents the angle between the direction of the perigee and the direction of the satellite.

The shape of the orbital plane is defined by its semi-major axis a and its eccentricity e. Its orientation in space is specified with the right ascension of the ascending node Ω and the inclination i. The position of a satellite in the orbital plane at a particular time is represented with the parameter of the true anomaly v.

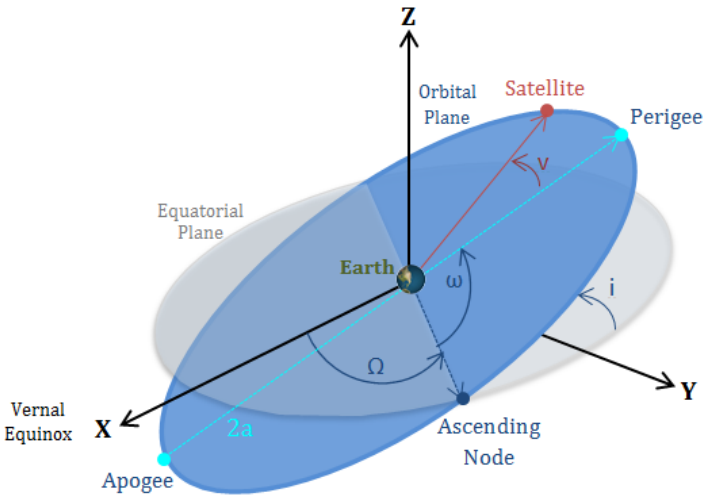

Figure 2.2: Keplerian elements.[1]

2.2.2. System description

When the Galileo space segment is fully operational, it will in total consist of 30 satellites in three Medium Earth Orbit (MEO) at an altitude of 23 222 km. Six of these satellites are spare ones. Each of the three orbital planes is inclined at an angle of 56 degrees to the equator, has a nominal semi-major axis of 29 599,8 km and is with a very small eccentricity almost circular.[1]

It takes the satellites 14 hours and five minutes to orbit the Earth. The orbit's high altitude ensures a high visibility of the satellites and its inclination a good coverage of polar latitudes. The trace on Earth will repeat itself after ten days during which the satellite completed seventeen revolutions. Additionally to these 24 active Galileo satellites exist two more, which are in a lower and elliptical orbit.

The Galileo satellites form a so-called Walker constellation. The geometry of such a Walker constellation is described with the three parameters $t/p/f$, where t represents the total number of satellites, p the number of orbital planes and f the relative spacing between satellites in neighbouring planes. Multiplying the parameter f by $360/t$ gives the difference of true anomaly in degrees for equivalent satellites in adjacent planes. Galileo is a 24/3/1 Walker constellation, which means that is consists of 24 active satellites in three orbital planes and the relative spacing between the satellites in neighbouring planes amounts to 15 degrees.

In each orbital plane will be eight active satellites evenly spread around and two further satellites on stand-by which can replace any failed satellite within the same plane. This replacement can be done within days by moving the spare one instead of launching a new one.

Figure 2.3 visualizes the Galileo constellation with its three orbital planes spaced by 120 degrees to each other. The satellites within a plane are separated with an angular distance of 45 degrees.

[1] https://www.gsc-europa.eu/system-service-status/orbital-and-technical-parameters

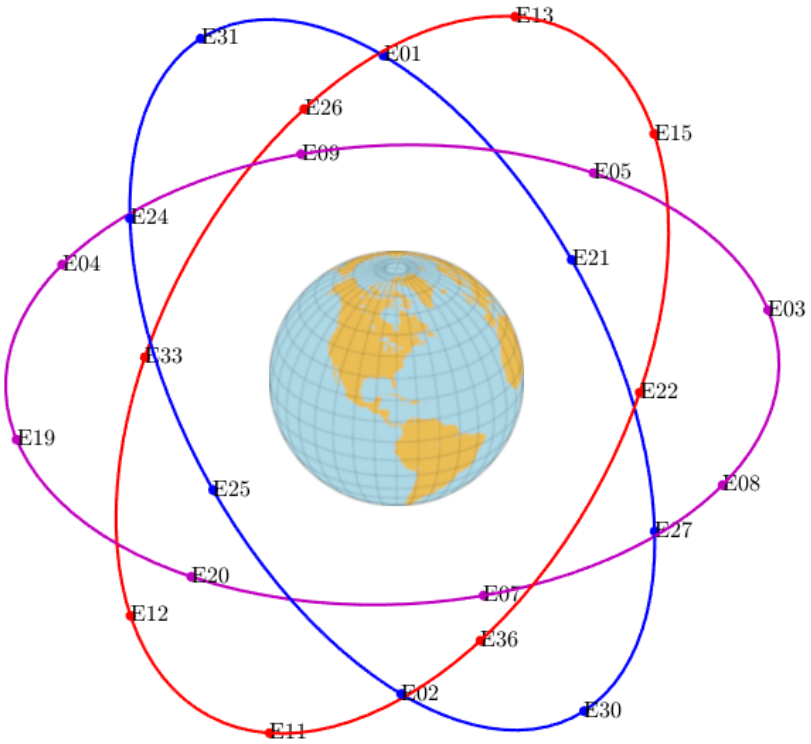

Figure 2.3: The Galileo constellation consisting of three orbital planes inclined at an angle of 56 degrees to the equator and spaced by 120 degrees to each other.

Figure 2.4 shows the configuration of the satellites in the three orbital planes. The 120 degrees spacing between the planes can be recognized in terms of the relative Right Ascension of Ascending Node (RAAN) which represents the angle between the vernal equinox and the ascending node of the orbital plane. The angular distance between the satellites within a plane and the relative phase shift factor of 15 degrees between satellites in equivalent slots in neighbouring planes can be recognized in terms of relative mean anomaly. The relative mean anomaly corresponds to the angular distance from the perigee which the satellite would have if it is moving in a circular orbit in the same elapsed time since it passed the perigee. Therefore, the mean anomaly always increases linearly with time.

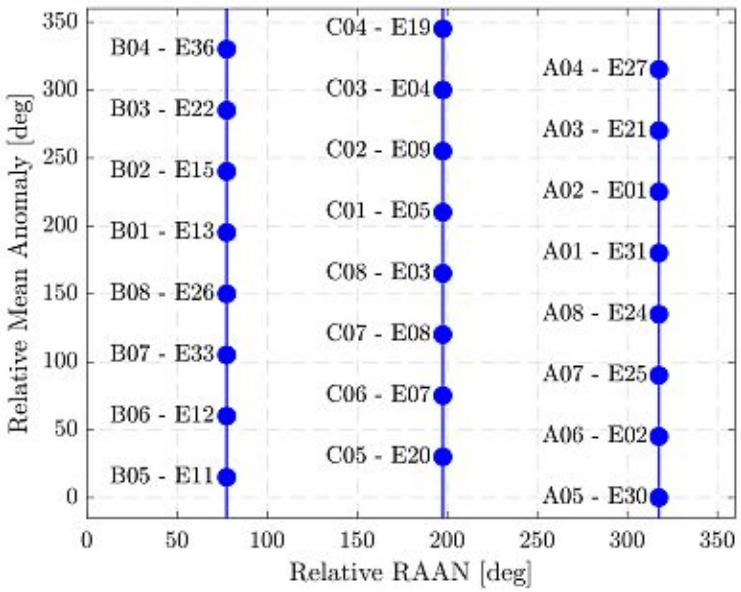

Figure 2.4: The three orbital planes of the Galileo space segment with eight satellites per plane. The satellites are indicated by its Space Vehicle Identifier (SV ID) and its slot assignments.

3. Satellite observations with VLBI

3.1. Applications

The following section focuses on new scientific applications which are offered by extending the VLBI research with observations to geodetic satellites such as the direct determination of the absolute orientation of the satellite constellation with respect to the ICRF, see section 3.1.1. Further, observations to satellites with VLBI antennas provide space ties which allow connecting the reference frames of the different space-geodetic techniques with high precision instead of using local ties. Section 3.1.2 provides an overview of the ITRF and the different aspects of local ties and space ties.

3.1.1. Determination of absolute orientation of satellite constellation

GNSS are highly insensitive to UT1-UTC due to the correlation of these parameters with the ascending node of the satellite orbit. An offset in UT1 can be fully absorbed by a shift of the Right Ascension of the Ascending Node (RAAN) of the satellite orbit without affecting the ranges between the stations and the satellites. Therefore, only their temporal derivatives, Length of Day (LOD) and nutation rates, can be determined with GNSS as the orbital parameters are assumed to be accurate enough over one day.

Thus, using the observations from GNSS ground stations only provides GNSS satellite orbits oriented with respect to the ground station network. That is why UT1-UTC time series are inserted from external sources in the orbit determination process to orient the tracking GNSS station network with respect to the ICRF. These time series are usually obtained from the IERS Bulletin A which relies on VLBI observations to quasars (Belli, 2020).

As VLBI stations can be oriented with respect to the ICRF by observations to quasars this can be used to determine the absolute orientation of the satellite constellation with respect to the ICRF directly by observing geodetic satellites equipped with a VLBI transmitter.

3.1.2. Terrestrial Reference Frame

Global reference systems are fundamental for many technical applications like navigation, surveying, global change monitoring and for reliable geodetic products. These coordinate systems are a reference for all kinds of measurements on and around the Earth. The most important system rotating with the Earth, the realization of a global TRF is the

International Terrestrial Reference Frame (ITRF), with the latest release denoted as ITRF2014 (Altamimi et al., 2016).

A new realization of the ITRF is published every three to five years and has improved compared to the preceding realization due to the larger amount of available observations as well as better strategies for the combination of ITRF. The ITRF2014 is a combined product of the four space-geodetic techniques namely VLBI, SLR, DORIS and GNSS.

It is possible to determine a TRF from only VLBI observations, the VLBI TRF, except the definition of the origin, this is defined only from SLR. However, a combined product is better because it is possible to use the strengths and to overcome the limitations of each space-geodetic technique.

In order to combine the independent single-technique solutions of the four space-geodetic techniques to one solution the technique-specific frames need to be related to each other. This is done introducing so-called local or space ties, whose concept is illustrated in Figure 3.1.

Local ties

The different geodetic instruments at a core site, a site with two or more space geodesy instruments which are observing at very close locations, can be connected by carrying out local surveys (distance and direction measurements and leveling) or using Global Positioning System (GPS) techniques to determine the 3d-coordinate differences between the reference points of the individual antennas (Altamimi et al., 2016). These terrestrial determined ties are commonly referred as local ties and are expressed as a set of coordinates in the ITRF. The proper weighted local ties are in addition to the observations of the space-geodetic techniques used for the ITRF combination (Altamimi et al., 2016) and relate the different techniques to each other.

Despite the precision of the surveys, the accuracy of the local ties varies between the different core sites and reaches an accuracy of centimetre level, according to (Altamimi and Ray, 2004) and (Altamimi et al., 2016). Deviations of up to a few centimetres occur when comparing the local ties and tie vectors derived from the estimates of the contributing space-geodetic techniques, shown by Seitz et al. (2012). The reasons for these discrepancies can be a local tie out of date, errors during the measurements, or missing variance covariance information, which is needed for the weighting.

Another challenge of determining the local ties represents the inaccessibility of the physical reference points of the antennas. Therefore, the survey of local ties is a difficult task and it is a large effort to determine local ties with a sufficient accuracy.

Space ties

The combination of space-geodetic techniques can be broadened by observing the same satellite with several techniques. This satellite is equipped with technique specific instruments, a retro reflector for SLR, a DORIS receiver, a GNSS receiver and a signal transmitter for S/X-band to enable observations with all four space-geodetic techniques. It therefore represents a so-called co-location in space.

Assuming the vectors between the satellite center of mass (COM) and the reference points of the different sensors are known with high precision, this configuration combines the different technique-specific frames. The combination can be done either on the satellite by comparing the positions of the satellite determined from observations of the different techniques or by determining the positions of the antennas on Earth in the satellite system (Plank, 2013).

These geometrical connections on a satellite level are referred as space ties. Space ties can be used to complement the ground based local ties which are established at co-location sites. The co-location satellite represents a reference point orbiting the Earth and all stations observing this satellite take part in the determination of space ties and in the combination of the different technique-specific frames.

Two satellite missions which would have realized this concept of a co-location satellite are GRASP (Geodetic Reference Antenna in Space; Nerem et al., 2011) and E-GRASP/ Erastosthenes (European Geodetic Reference Antenna in Space; Biancale et al., 2017), which were proposed to NASA and ESA respectively, but were rejected.

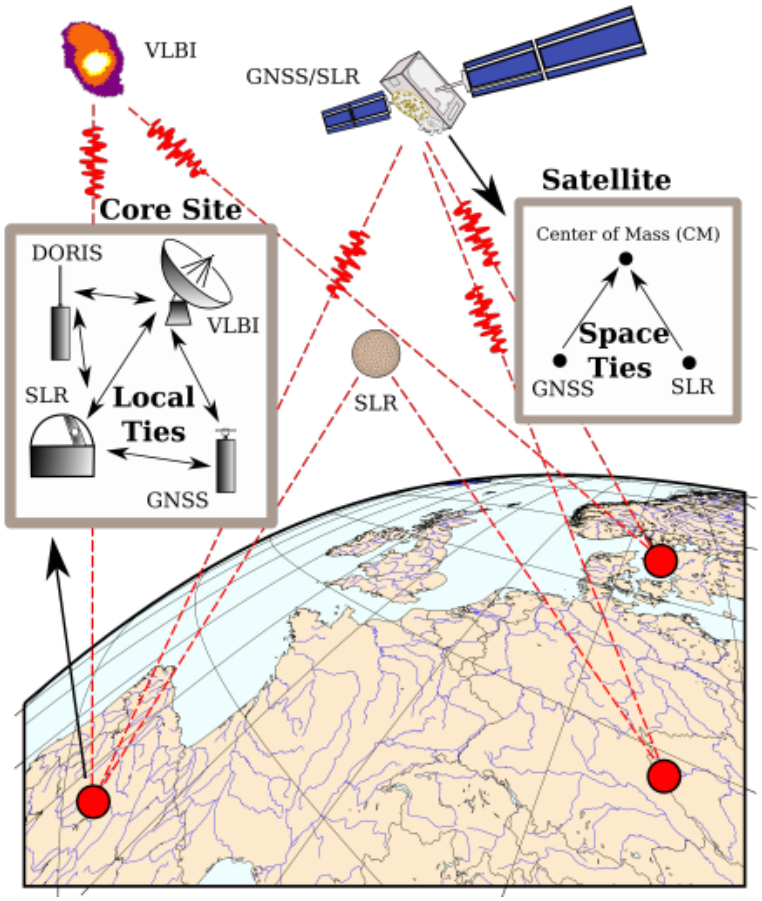

Figure 3.1: Concept of local ties and space ties, taken from Klopotek (2020).

3.2. Scheduling of Satellite Observations

As already mentioned in section 2.1.2, scheduling is a complex process which becomes even more complex including observations to satellites and near-field targets in general. Because the objects are close to Earth the signal is not arriving in planar waves on Earth and a cross-eyed observation configuration has to be considered, as illustrated in Figure 3.2. The source position, right ascension and declination in a topocentric equatorial system, is different at different sites. Due to the fact that a satellite is moving in its orbit it is not longer stationary on the sky and its position is changing over time. In order to observe it, the antenna has to move during the observation and therefore change its pointing direction over time. This can be challenging for large antennas due to their rather slow antenna slew rates, especially observing satellites with low altitudes as they are moving faster.

These aspects indicate that observations to satellites have additional requirements for

being feasible. In order to schedule an observation to a satellite the common visibility from the observing antennas, the exceedance of the antenna slew rates, the satellite's distance to the Sun and the cable wrap have to be checked. Usually the conditions, visibility, cable wrap and Sun distance are checked once per scan but as the satellite is moving and its position is changing these conditions have to be checked continuously during a scan.

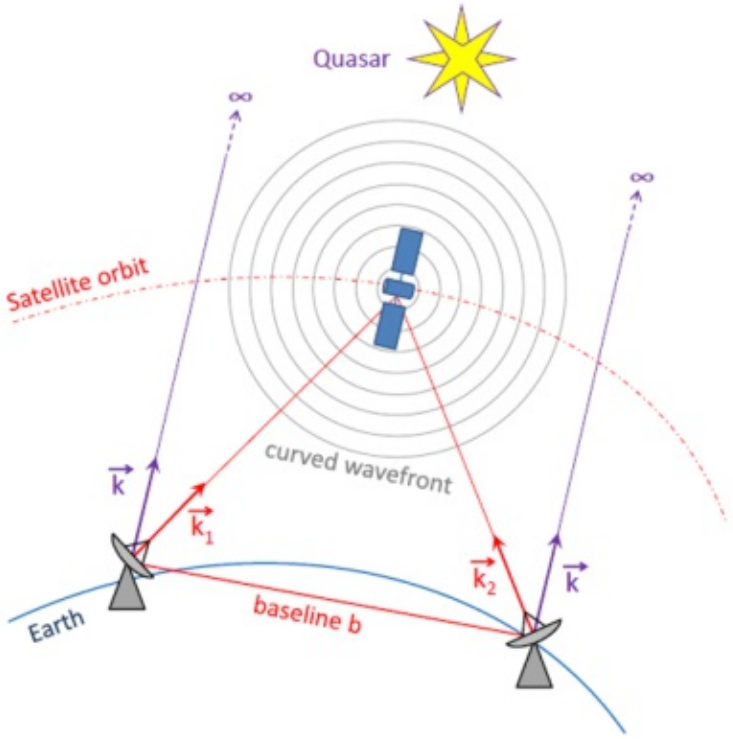

Figure 3.2: Geometry of observations to satellites, from Hellerschmied (2014). As a result of the short distance of the satellite to Earth, the signal arrives curved and therefore the view directions between stations at different locations are different $\vec{k}_1 \neq \vec{k}_2$. If the stations point to a quasar, their view directions $\vec{k}$ are equal.

3.2.1. Visibility

In order to carry out VLBI observations to a target, it has to be visible from all participating stations. A satellite is visible from an individual station if it is above the horizon and therefore visible under a positive elevation angle. If the satellite is seen under a negative elevation angle, it means that the Earth is in between and it therefore cannot be observed. Sometimes a mountain, a building or another object is blocking the

view and a target is not visible in certain areas although it is above the horizon. The information about the visible areas from a station is stored in so-called horizon masks.

There is not a horizon mask defined for each station but to avoid observations close to the horizon which could cause reaching the hardware limits of the antenna axis a so-called cut-off elevation angle is set. This angle defines the minimum elevation angle which can be scheduled, typically five degrees. If the satellite is above the horizon but below the cut-off elevation it is visible but does not meet the condition and therefore cannot be scheduled. In VieSched++ this value can be set individually for each station and source (Schartner, 2019). Figure 3.3 illustrates the horizon mask for the station AGGO and WETTZ13N.

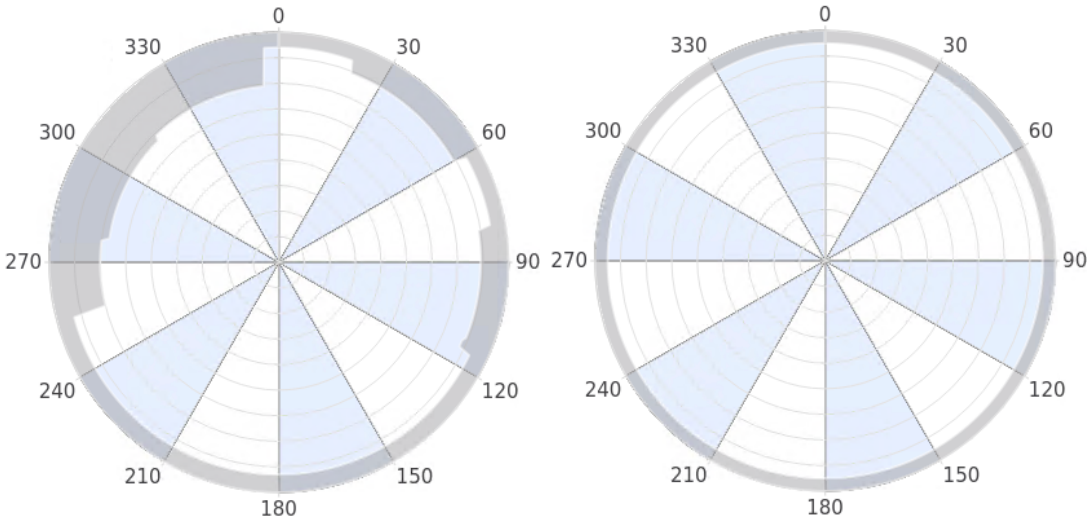

(a) (b)

Figure 3.3: Horizon masks for station (a) AGGO and (b) WETTZ13N. The mask of AGGO shows parts where the view is blocked up to an elevation of more than 20 degrees while the horizon mask of WETTZ13N shows a cut-off angle of five degrees for all azimuth directions.

The common visibility of a satellite by multiple stations is dependent on the baseline lengths between the participating stations and the height of the satellite. There was a visibility study carried out by Plank (2013). The area where the satellite is visible for two stations is becoming smaller with increasing distance between the stations. Satellites in orbits with higher altitude are easier visible than satellites in lower orbits.

3.2.2. Antenna slew rates

The VLBI telescopes included in the current IVS network have antenna slew rates in the range from 0.4 degrees/sec to 3 degrees/sec (Plank, 2013). VLBI antennas built according to the VGOS specifications have a smaller diameter of their dish, about 12 meters, but they are therefore faster with slew rates in the range from 6 degrees/sec up to 12 degrees/sec (Schuh and Behrend, 2012).

During the observation of extragalactic sources the pointing direction of the telescope has only be adjusted due to the rotation of the Earth. This correction results in maximum to 0.25 degrees/min.

If satellites are observed the demands on the slew rates of the antenna are higher as the satellite is moving much faster while observing it. The appearing speed of the satellite for a site on the Earth's surface is dependent on the altitude of the satellite and on the elevation of the antenna at which the satellite is observed. Satellites in low orbits are moving faster than satellites in orbits with a high altitude. If the satellite is observed at low elevations the satellite's position seen from Earth is changing slowly and therefore the pointing direction of the antenna only has to change slowly in order to follow it. But if the satellite is visible at high elevations the rate of changing of the elevation angle is high and the antenna has to move fast in order to follow the satellite. The most challenging observations are observations to satellites in low orbits overpassing close to the zenith.

There are three different antenna mount types used for VLBI telescopes, the azimuth-elevation mount (AzEl), the equatorial mount (HaDec) and the X-Y mount. Each of these mount types shows areas, so-called keyholes, at which the coordinate of one axis is undefined for a certain antenna pointing direction and therefore coordinate singularities occur. For example, at AzEl mount antennas the azimuth is not defined for an elevation of 90 degrees. The antennas are able to point at directions within the keyholes, but they are not able to follow the satellite through these positions. In the following the different antenna mount types are described, according to Salzberg (1967).

Azimuth-Elevation mount (AzEl)

Telescopes with large dishes usually have an azimuth-elevation mount. This mount type has a fixed vertical axis (azimuth axis) and a moving horizontal axis (elevation axis) which is attached to the platform that rotates about the fixed azimuth axis. The azimuth motion is typically larger than 360 degrees in a range from $\pm$ 270 degrees relative to either North or South and the elevation motion is usually in a range from five de-

grees to 85 degrees (Petrachenko, 2013). As it can be seen in Figure 3.4 the keyhole for this mount type occurs in zenith direction (in this example with 10 degrees diameter). This means that within this keyhole coordinate singularities and maximum azimuth rates occur and a station is not able to follow a satellite passing through this area. For example, if a satellite is overpassing an AzEl mount antenna through the zenith, the station would have to turn 180 degrees instantaneously in azimuth direction to follow the satellite. This would require an infinite slew speed of the azimuth axis and therefore it is impossible to track a satellite overpassing a station in zenith.

Equatorial mount (HaDec)

This antenna mount type has a fixed axis in the direction of the celestial pole, the equatorial axis, and a moving axis perpendicular to the equatorial axis, the declination axis. The covered area is dependent on the latitude of the site but in general it is less than ± 180 degrees for the equatorial axis and less than ± 90 degrees for the declination axis (Petrachenko, 2013). The advantage of this mount type is that for tracking a fixed point in space and setting the declination, it is only necessary to drive the hour angle to compensate the Earth's rotational rate (Salzberg, 1967). The limited area where a satellite cannot be tracked with this mount type, the keyhole, is in direction of the celestial pole, see Figure 3.4. In this direction, at a declination of 90 degrees, the hour angle is not defined.

X-Y mount

Antennas with a X-Y mount type are mainly used for satellite tracking due to the possibility of tracking through the zenith. This antenna positioner consists of two perpendicular axes, the X and Y axis. The fixed axis points to the horizon and is either aligned to the North-South direction (XYNS mount) or the East-West direction (XYEW mount). Two keyholes occur on the horizon, in the North and South or in the East and West, dependent on the direction of the fixed axis, where the satellite tracking is not possible, as it can be seen in Figure 3.4.

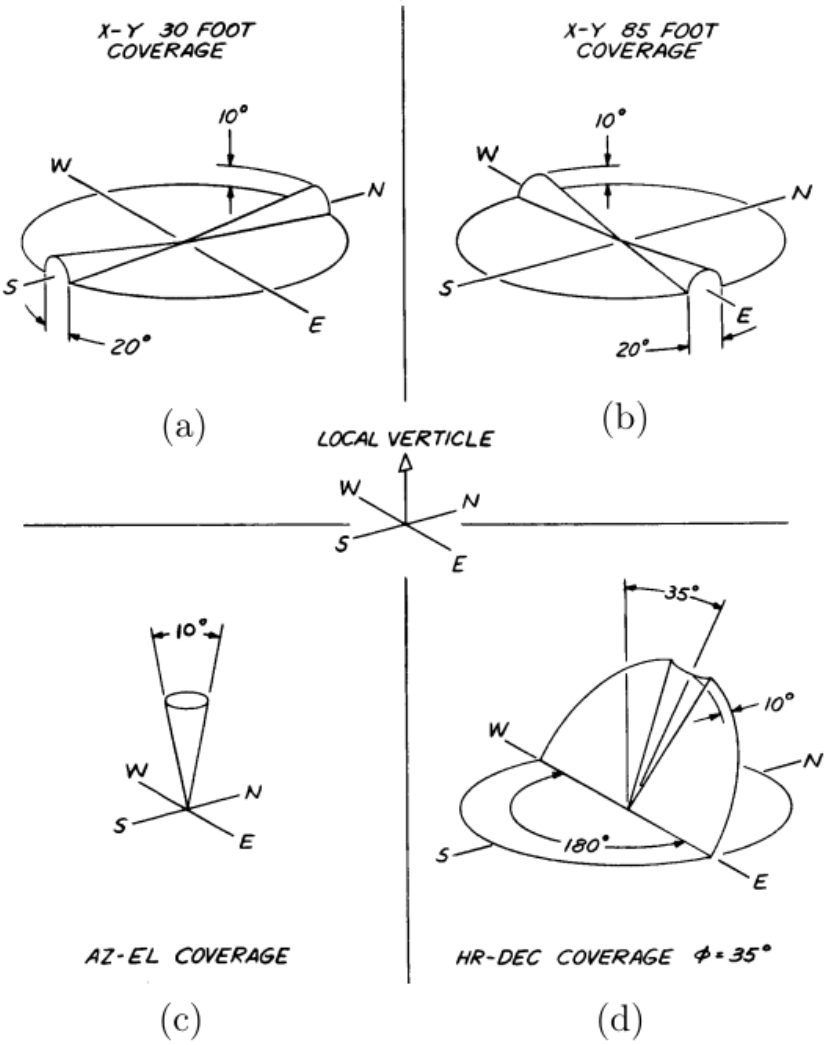

Figure 3.4: Keyholes for the different VLBI antenna mount types (a) XYNS mount, (b) XYEW mount, (c) AzEl mount and (d) HaDec mount for an antenna located at geographical latitude of 35 degrees, in which coordinate singularities occur and therefore a tracking of a satellite is not possible, adapted from Salzberg (1967).

3.2.3. Sun distance

The Sun is emitting strong radiation which could lead to signal corruption, making the recorded data useless, or even to some technical damage of the receiver hardware by pointing directly to it. In order to avoid this the angular distance between the observed target and the Sun has to be considered during the observation and has to be greater than a defined threshold.

3.2.4. Cable wrap

Cable wrap is only relevant for AzEl antennas, which rotate around the azimuth axis. The cable is connected to the equipment which is fixed to the ground and slewing always to the same direction would therefore lead to a twist around the mount. In order to avoid this and to check if the antenna is reaching its cable wrap limits while slewing to the next source and to determine the slew times between following scans it is important to track the cable wrap position (Schartner, 2019). Considering observations to satellites it is also necessary to monitor the cable wrap while following a satellite during a scan as the azimuth angle can change quickly for satellites in low orbits. Additionally, it is needed to check the cable wrap position to start a satellite scan in the correct segment to allow the antenna following the satellite until the end of the scan without reaching the cable wrap limits (Hellerschmied, 2018). The antennas usually have a cable wrap bigger than 360 degrees which allows a more flexible scheduling and slewing. Figure 3.5 visualizes the cable wrap for WETTZ13N with limits of -90 degrees and 450 degrees which allows the antenna to turn in total 540 degrees. The cable wrap is divided in three parts. The counter-clockwise cable wrap (ccw) section starts at the lower limit and covers the overlapping azimuth ranges. It is followed by the neutral (n) section until the azimuth ranges overlap again and the clockwise cable wrap (cw) section starts until the cable wrap reaches the upper limit. The cable wrap position for an antenna pointing in the azimuth directions within the overlapping areas is ambiguous as the antenna can be located either in the ccw or in the cw cable wrap section. It is therefore important to monitor the cable wrap position of the antenna in order to avoid to exceed the limits.

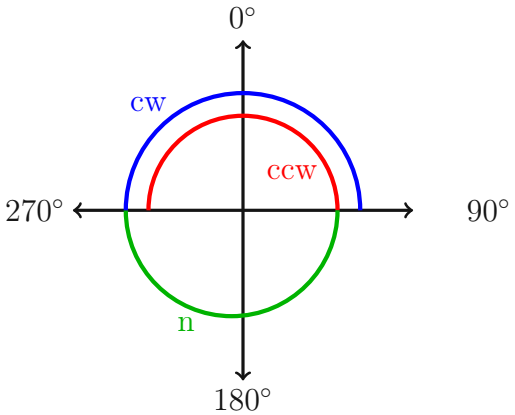

Figure 3.5: Cable wrap of the station WETTZ13N with color-coded cable wrap sections. For the azimuth values in the range from 270 to 360 degrees and from 0 degrees to 90 degrees the antenna can be either located in the counter-clockwise (ccw) or clockwise (cw) cable wrap section.

3.3. Satellite Orbit Prediction

The determination of the position of a satellite at a specific time requires predicted satellite orbits. The knowledge of the exact position of a satellite is important and is needed in two steps requiring different accuracy demands. First, in order to carry out the scheduling but also later to calculate the pointing direction of the antenna to observe and track the satellite properly, see section 3.3.1. The different sources providing orbit predictions are discussed in section 3.3.2 and the orbit propagation used in the satellite scheduling module of VieSched++ is described in section 3.3.3.

3.3.1. Accuracy of Orbits

There are different requirements concerning the accuracy on the satellite positions for scheduling and tracking. In the scheduling process the satellite positions are used to do the observation planning. It is determined if a satellite is visible from a station network or not and if the requirements for a feasible satellite observation, see section 3.2, are fulfilled. Therefore, the accuracy demands on the satellite position for scheduling are not that critical and rather low compared to the requirements for tracking.

The satellite positions which are used for calculating the pointing data of the antennas for tracking have to be of high accuracy in order to point the antenna accurately on the satellite during the observation.

3.3.2. Data Formats

Orbit predictions are needed for determining the satellite position in the future. There are several sources providing orbit predictions in different data formats for different satellite constellations. Orbit predictions are provided by the International GNSS Service (IGS) as Standard Product 3 (SP3) files (Spofford and Remondi, 1995), by the International Laser Ranging Service (ILRS) (Pearlman et al., 2002) in the Consolidated Prediciton Format (CPF) (Ricklefs, 2006) and by the North American Aerospace Defence Command (NORAD) as Two-Line Element (TLE) data.

SP3 files Different orbit products are distributed by the IGS in the SP3 file format, which allow the calculation of the satellite orbits with high precision. But there are two downsides of using SP3 files. The data is not available for all GNSS satellites and it is available only with a delay which makes it suitable for post-processing but not useable for orbit predictions to the future.

CPF files The ILRS is providing orbit predictions in the CPF file format which are usually used for satellite tracking with SLR. The files provide daily tables of x, y and z positions for the tracked satellites which can be interpolated predictions with a high degree of accuracy. The prediction file for a satellite contains data for several days, usually with predictions for four days from the day of release. The integration of satellite positions weeks and months after the epoch of the last entry is associated with an increasing loss of accuracy but enables the use of scheduling, which requires only limited accuracy, for several weeks in the future. The downside of this data format is the limited availability as it is only available for satellites which are part of the ILRS observing program.

TLE data In the file formats discussed above, SP3 and CPF, the satellite orbit data is provided as time sequences of satellite positions in cartesian coordinates (x, y, z) at certain epochs. This makes time-consuming integrations necessary to predict the satellite position at a particular time in the future.

The NORAD provides orbit predictions in the TLE format which contains the mean Keplerian orbital elements at a particular epoch plus additional parameters allowing the modeling of certain perturbing forces. This makes it possible to use them for orbit predictions without time-consuming integrations. The position and velocity of a satellite at a specific time is determined by applying a prediction formula on the TLE data, which is described in section 3.3.3. The advantage of TLE datasets is the public availability for thousands of space objects on the website CelesTrak[2]. This means that there is almost no limitation on the selection of satellites observing with VLBI telescopes because the TLE data is available for all Earth satellites.

3.3.3. Orbit propagation with TLE Data

To estimate the position and velocity of the space object at a specific time the corresponding TLE element set needs to be propagated using perturbation models, Simplified General Perturbation (SGP) or Simplified Deep Space Perturbation (SDP). These models predict the effect of perturbations caused by the shape of the Earth, the atmospheric drag and the gravitational effects of the moon and Sun and model the motion of the satellite on its orbit around the Earth.

There are five models for predicting satellite positions and velocities available - SGP,

[2]https://www.celestrak.com/NORAD/elements/

SGP4, SDP4, SGP8 and SDP8. These models are compatible with the TLE data and therefore the NORAD TLE data sets have to be used with one of the models in order to achieve the maximum prediction accuracy. The different models are described in (Hoots and Roehrich, 1980). Currently, the NORAD TLE data sets are generated using either the SGP4 or the SDP4 model, depending if the space object is near to the Earth or in deep space (Hoots and Roehrich, 1980). The SGP4 model is used for predictions for space objects near the Earth, objects with a round-trip period of less than 225 minutes. The SDP4 model is the deep-space model and is used for the other objects with a round-trip period greater or equal than 225 minutes. Assuming a circular orbit, a period of 225 minutes corresponds to an altitude of 5877 km. It is necessary to distinguish between the two models as the modelled perturbation influences are dependent on the altitude of the orbit.

4. Method

This section gives an overview about the basic program concepts of the new satellite scheduling module in VieSched++. The main calculations and transformations for determining the visibility of a satellite from an individual station are described using the C++ SGP4[3] library, see section 4.1. Further, based on the time periods a satellite is visible for the individual stations of a network, it is outlined how to derive potential observation periods during which the satellite is visible for at least two stations of the network simultaneously.

There are two different possibilities for scheduling observations to satellites using VieSched++. First, the semi-manual scheduling approach and second, the automatic mode, see section 4.2.2 and 4.2.3 respectively.

4.1. Visibility of a satellite

In the following the approach for determining the visibility of a satellite by computing the view angles of an antenna pointing in the direction of the satellite is described. In a first step, the cartesian position of the satellite and the station are calculated in the Earth-Centered Inertial coordinate system (ECI) and further used to determine the looking angles of the antenna observing the satellite.

4.1.1. Satellite position as ECI coordinates

In VieSched++ the C++ SGP4[3] library is used to predict satellite positions based on TLE datasets. This library contains the equations and the source code to predict satellite positions using the SGP4 model. This results in a cartesian position, equation 4.1, and velocity vector versus time since the TLE epoch in the Earth-Centered Inertial "true equator, mean equinox" (ECI TEME) coordinate system (Vallado, 2013). A detailed description of the ECI coordinate system can be found in section A.1.

$$\vec{r}_{\text{sat}} = \begin{pmatrix} x \\ y \\ z \end{pmatrix}_{ECI} \tag{4.1}$$

[3]https://www.danrw.com/sgp4/

4.1.2. Station position as ECI coordinates

The positions of the stations are available in terms of ITRF coordinates (X, Y, Z) and in geographic coordinates (λ, ϕ, h) in an Earth Centered Earth Fixed (ECEF) frame. For further calculations, the site's position has to be converted to the same reference frame as the satellite position and it is therefore converted from geographic coordinates to coordinates in the ECI system. This transformation is represented in the equations 4.2 - 4.4. It is necessary to determine the angle between the Greenwich Meridian and the direction of the vernal equinox, the Greenwich Sidereal Time GST and further θ which corresponds to the angle between the observer's longitude and the vernal equinox, the local sidereal time. In order to approximate the Earth as an oblate spheroid, the radius of curvature, N_{H}, is calculated in equation 4.3 using R, the Earth's equatorial radius and f, the Earth oblateness flattening factor. Further, the cartesian ECI coordinates can be determined with equation 4.4.

$$\theta = GST + \lambda \tag{4.2}$$

$$N_{\mathrm{H}} = \frac{R}{\sqrt{(1 - f(2 - f) \cdot sin^2(\phi))}} \tag{4.3}$$

$$\vec{r}_{\mathrm{stat}} = \begin{pmatrix} (N_{\mathrm{H}} + h) \cdot cos(\phi) \cdot cos(\theta) \\ (N_{\mathrm{H}} + h) \cdot cos(\phi) \cdot sin(\theta) \\ (N_{\mathrm{H}} \cdot (1 - f)^2 + h) \cdot sin(\phi) \end{pmatrix}_{ECI} \tag{4.4}$$

4.1.3. View angles

Now, the geocentric space fixed position vectors of the satellite $\vec{r}_{\mathrm{sat}}$ and the station $\vec{r}_{\mathrm{stat}}$ are available in the ECI system. These vectors can be used to determine the looking angles of the station, in terms of azimuth and elevation, when pointing in the direction of the satellite. Therefore, the satellite's position is determined in the topocentric horizon coordinate system, SEZ, see section A.2. This system moves with the Earth and has its origin at the location of the station on the Earth's surface, illustrated in Figure 4.1. It allows to define look angles in terms of azimuth (β) and elevation (el) of a station observing a satellite.

First, the origin of the satellite vector is moved to the station's location by calculating the difference vector $\vec{r}_{\mathrm{d}}$ and further the coordinates of the satellite's position in this

system are determined with equation 4.6, where ϕ represents the station's latitude and θ the local sidereal time. Finally, the azimuth (β) and elevation (el) angle can be obtained with the formulas 4.7 and 4.8 (Vallado, 2013). Concerning the azimuth angle, it has to be ensured that the correct quadrant is selected for the arctangent.

$$\vec{r}_{\mathrm{d}} = \vec{r}_{\mathrm{sat}} - \vec{r}_{\mathrm{stat}} \tag{4.5}$$

$$\vec{r}_{\mathrm{SEZ}} = \begin{pmatrix} r_{\mathrm{S}} \\ r_{\mathrm{E}} \\ r_{\mathrm{Z}} \end{pmatrix} = \begin{pmatrix} sin(\phi)cos(\theta) & sin(\phi)sin(\theta) & -cos(\phi) \\ -sin(\theta) & cos(\theta) & 0 \\ cos(\phi)cos(\theta) & cos(\phi)sin(\theta) & sin(\phi) \end{pmatrix} \cdot \begin{pmatrix} r_{\mathrm{d,x}} \\ r_{\mathrm{d,y}} \\ r_{\mathrm{d,z}} \end{pmatrix} \tag{4.6}$$

$$el = asin\Big(\frac{r_{\mathrm{Z}}}{|\vec{r}_{\mathrm{SEZ}}|}\Big) \tag{4.7}$$

$$\beta = atan\Big(-\frac{r_{\mathrm{E}}}{r_{\mathrm{S}}}\Big) \tag{4.8}$$

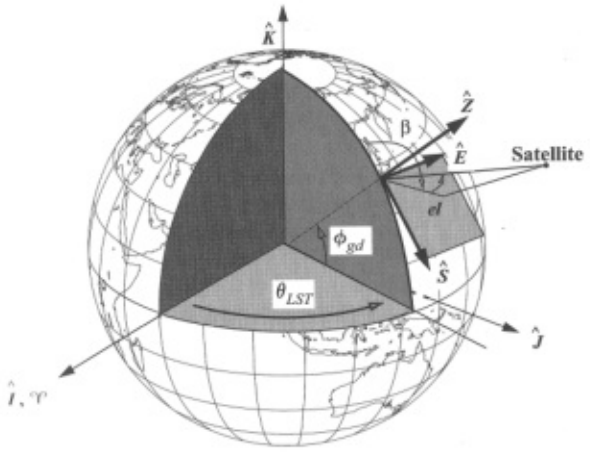

Figure 4.1: Topocentric Horizon Coordinate System, SEZ, which moves with Earth and has its origin on the Earth's surface, taken from Vallado (2013). The local sidereal time θ_{LST} and the geodetic latitude ϕ_{gd} are used to orient the system to a fixed location.

The azimuth and elevation angle are now used to check whether the satellite is visible for the station or not. This is dependent on the horizon mask of the station. If there is not any horizon mask available for the station the satellite has to be above the defined cut-off elevation.

4.2. Satellite Scheduling with VieSched++

VieSched++ is a new VLBI scheduling software, which is flexible and easy to use. It is written in C++ and has a modern Graphical User Interface (GUI). It allows to create schedules with observations to radio sources of highest quality making use of several optimization criteria (Schartner, 2019). One missing feature of VieSched++ is the option to schedule observations to satellites. Due to the success of previous satellite observation missions a satellite scheduling module was implemented in VieSched++.
VieSched++ provides two possibilities for including observations to satellites in a schedule. It can be done in a semi-manual or automatic mode.

Semi-Manual approach

The semi-manual scheduling approach allows the user to investigate the satellites of interest and to select the satellite scans using the GUI of VieSched++. The user is supported in his decisions by graphically presented information of the different satellites, like the ground track of the satellite and elevation plots. The user can select a satellite and the module determines all possible observation periods from the defined station network, considering several observation conditions. Further, the scheduler can select scans and add them to the schedule as a-priori scans. In the second phase the remaining part of the schedule will be filled with observations to quasars. The advantage of the semi-manual approach is, that the user has full control over the added satellite scans which is important for development and research activities. The downside of adding satellite observations manually is, that it is time-consuming and requires experience of the user.

Automatic approach

The scheduling of observations to satellites can be done automatically without user interaction. In this approach the satellite is treated like a quasar and the scheduling is done using the general optimization algorithm. The advantage of this method is, that the schedule including satellite observations can be created fast and the user does not need much experience in terms of satellite observations. The disadvantage is, that the user has less control about the selected satellite scans.

In the following the two different approaches, semi-manual and automatic, are described. The necessary input data, the different procedures and the possibilities of the scheduler are explained.

4.2.1. Input data

For generating a schedule it is necessary to consider the different characteristics of the participating VLBI stations and the observed sources but also the observing modes which should be used. The VLBI antennas differ in terms of slew rates, sensitivity and cable wrap limits and the observed sources show differences in brightness and source structure. All these factors need to be considered during the creation of a schedule. The information about the antennas, the sources and the observing modes which should be used is stored in so-called sked catalogs (Vandenberg, 1999) and loaded by VieSched++ (Schartner, 2019).

The new possibility of satellite scheduling in VieSched++ requires information about the satellites which should be observed. In VieSched++ the orbit propagation is computed based on the TLE datasets of the satellites. The TLE datasets from the satellites of interest can be downloaded from dedicated websites and stored in a text file. This text file is loaded by VieSched++ and the included satellites appear in the GUI. In the GUI of VieSched++ the user has to select a station network and define the start time and duration of the session which should be scheduled.

4.2.2. Semi-manual Mode

The semi-manual satellite scheduling is carried out using the GUI of VieSched++. The user has the possibility to investigate the different satellites, select a satellite and add the satellite scans as a-priori scans to the schedule. In the following the possibilities of the user, the graphically represented information of the different satellites and the procedure of calculating the potential observation periods of a satellite are described.

Investigation of the different satellites

Before the user decides which satellite should be observed it is possible to investigate the different satellites which are loaded in VieSched++. All the information supporting the scheduler in his decisions is represented graphically in the GUI of VieSched++. The user has the possibility to consider the ground track of the satellite and to view the position of the satellite over Earth during the session, see Figure 4.2. Further, it is possible to examine the elevation angles over time under which a satellite is visible for the participating stations, illustrated in Figure 4.3. The module also provides information about the percentage of time of a session the satellite is visible from a certain number of stations, see Figure 4.4.

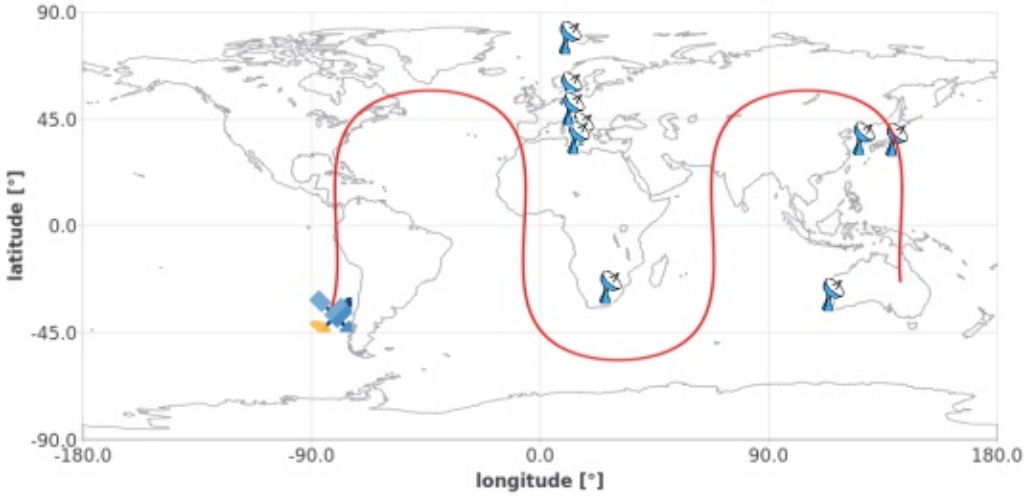

Figure 4.2: Ground track of the Galileo satellite E11 together with nine radio telescopes, which are visualized in Figure 5.1, during the 24-hour session IVS-R1978 on December 21, 2020.

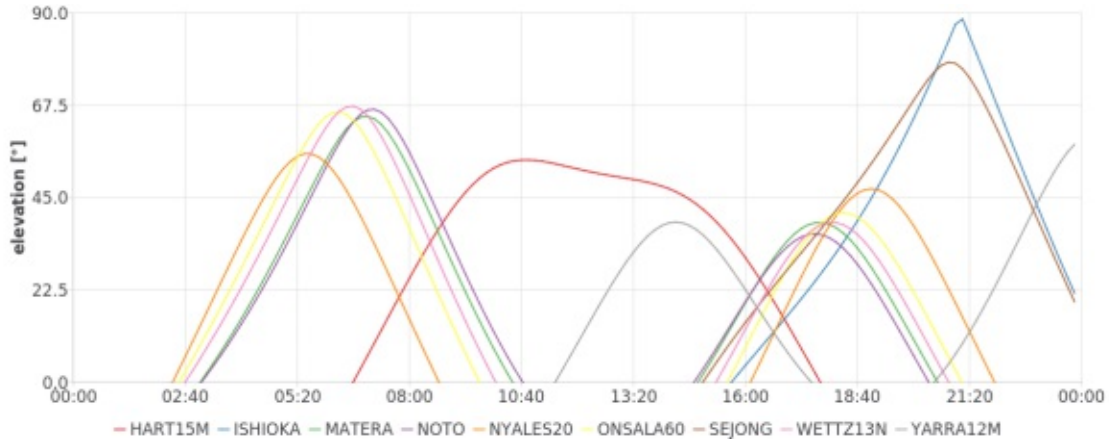

Figure 4.3: Elevation angles over time from all stations to Galileo satellite E11 during the 24-hour IVS-R1978 session on December 21, 2020.

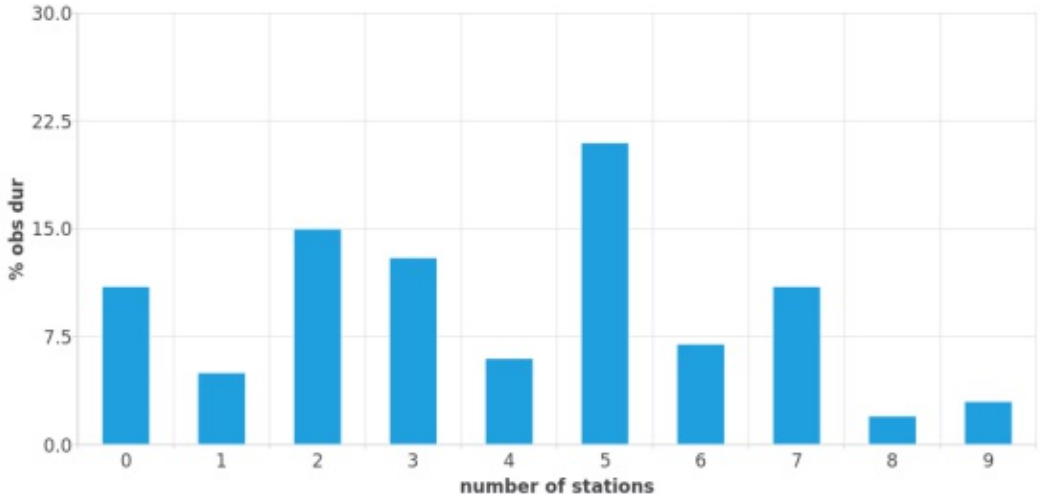

Figure 4.4: Percentage of time the Galileo satellite E11 is visible from a certain number of stations, during the 24-hour IVS-R1978 session on December 21, 2020 assuming a cut-off elevation angle of five degrees.

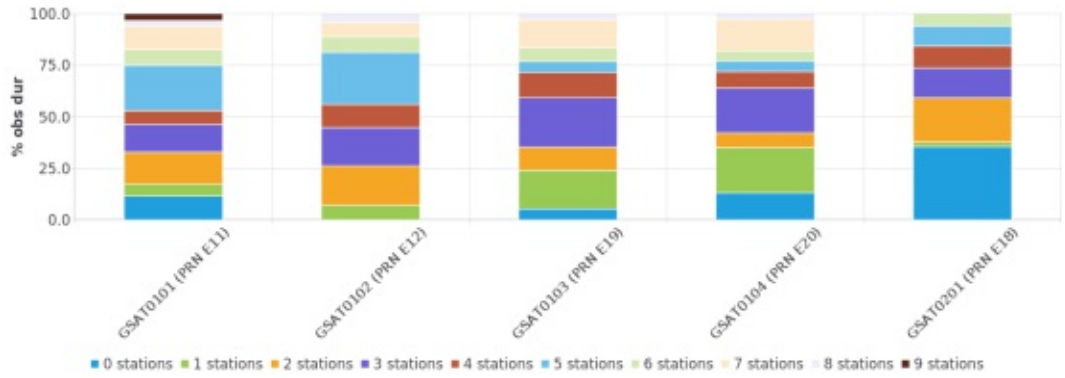

Figure 4.5: Visibility percentage for five different satellites during the 24-hour IVS-R1978 session on December 21, 2020 assuming a cut-off elevation angle of five degrees. The bar in the left shows the visibility for the Galileo satellite E11.

Determination of possible scans

When the user decided which satellite should be observed it is possible to calculate all possible scans with the selected station network. Section 4.1 describes the calculations and transformations which are necessary to determine the azimuth and elevation angle of an antenna pointing in the direction of a satellite and therefore determine whether a satellite is visible for a station or not. However, the visibility of a satellite for a station does not mean that the station is able to observe it. The conditions, which are necessary to be fulfilled that the satellite can be observed additionally to its visibility, are described in section 2.1.2 and are summarized briefly below.

- **Antenna slew rates:** To ensure that the station can follow the satellite in the sky, the slew rates of the antenna must not be exceeded.
- **Sun distance:** It is checked if the angular distance between the satellite and the Sun is above the defined threshold to avoid observations close to the Sun.
- **Cable wrap:** The cable wrap position is determined and monitored in order to avoid the antenna reaching its cable wrap limits.

A satellite is observable from one individual station if all these conditions are fulfilled simultaneously. This approach is carried out during the whole session to determine all possible time periods where the satellite is observable for all individual stations of the defined network.

The VLBI technique requires observations to the same satellite with a net of at least two telescopes at the same time, see section 2.1.1. Therefore, it is necessary to determine time periods where the satellite is observable from at least two stations of the network simultaneously. This is done by determining the overlapping time periods of the possible observation times of the individual stations, see Figure 4.6. During these overlapping time periods the satellite is visible from more than one station simultaneously. The time periods during which the satellite is observable for at least two stations are provided to the user as possible scans.

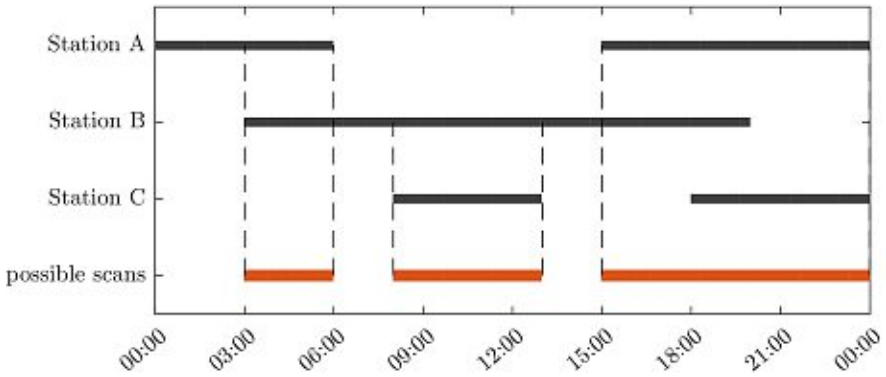

Figure 4.6: Determination of possible scans. The black bars indicate the time periods where the satellite is visible for the respective stations. The orange bars are obtained by determining the overlaps of the time periods of the individual stations and therefore represent time periods during which the satellite is visible for at least two stations.

Procedure fix scans

Once the scheduler selected one or more satellites all possible scans with the chosen network are determined. The user has the possibility to select a scan and adjust the start time and duration or remove a station from this scan. The selected scan is visualized by means of an elevation plot, elevation angles over time, see Figure 4.7, and a skyplot showing the satellite transits seen from the observing stations, see Figure 4.8. Finally, these scans can be fixed as a-priori scans to the schedule. The remaining part of the schedule is filled automatically with observations to quasars using the general optimization algorithm of VieSched++.

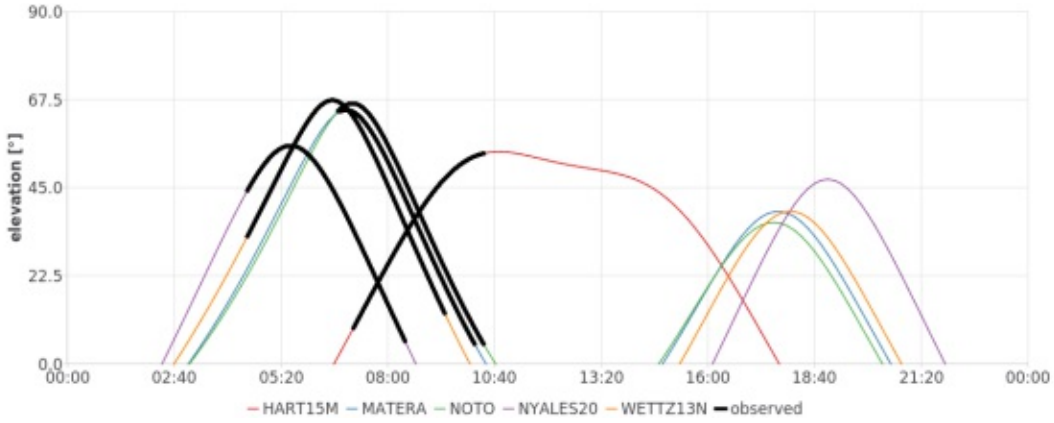

Figure 4.7: Elevation angles over time to Galileo satellite E11 from five of the nine stations in session IVS-R1978. The potential observation period of the satellite is highlighted in bold lines.

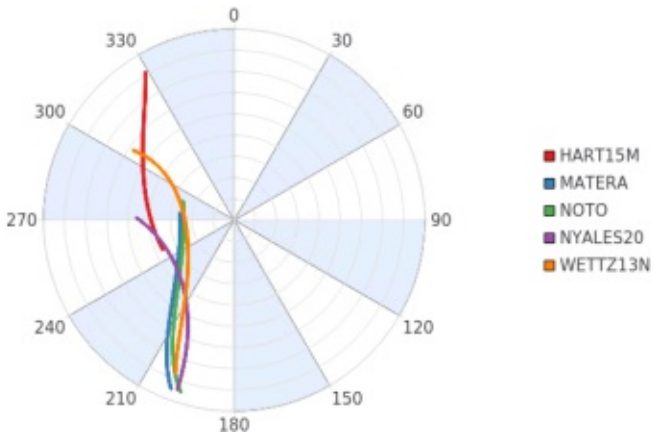

Figure 4.8: Skyplot with azimuth and elevation angles to Galileo satellite E11 from five of the nine stations for a possible scan in session IVS-R1978.

4.2.3. Automatic Mode

The automatic mode schedules observations to quasars and satellites automatically without user interaction. The satellite is treated like a quasar and the schedule is created scan by scan using the general optimization algorithm of VieSched++. All possible scans at the current scheduling time are created and compared using some metrics like improvement of sky coverage, the number of observations and total duration of the scan (Schartner, 2019). Based on the metrics, the best scan is selected. In order to increase the number of satellite scans in the schedule it is possible to give the satellites a higher weight than the quasars. This means that a satellite scan is preferred in the process of comparing all possible scans and selecting the best one.

5. Evaluation study of satellite observations

This chapter focuses on the visibility of Galileo satellites from the nine station network which was observing during the 24-hour IVS-R1978 session on December 21, 2020 at 00:00 UTC. The possible observation periods of a satellite from a VLBI network are determined using the newly developed satellite scheduling module in VieSched++. The possible satellite observations are evaluated through the number of stations from which the satellite is observable and by the observation geometry between the observed baselines and the position of the satellite.

5.1. VLBI network

In order to study the visibility of the Galileo satellites from a VLBI network, a so-called "rapid turnaround" IVS session was used to carry out the investigations. These sessions are observed on Mondays and Thursdays and are called IVS-R1 and IVS-R4, respectively. In this study the 24-hour IVS-R1978 session was chosen which was observed on December 21, 2020 at 00:00 UTC using a nine station network. Figure 5.1 depicts a map of the VLBI antennas participating in this session. This nine station network was used for the evaluation study of satellite observations. The network is located in the eastern part of the globe and most of the stations are located on the northern hemisphere, only two of them, Hartebeesthoek (HART15M) and Yarragadee (YARRA12M), are located on the southern hemisphere.

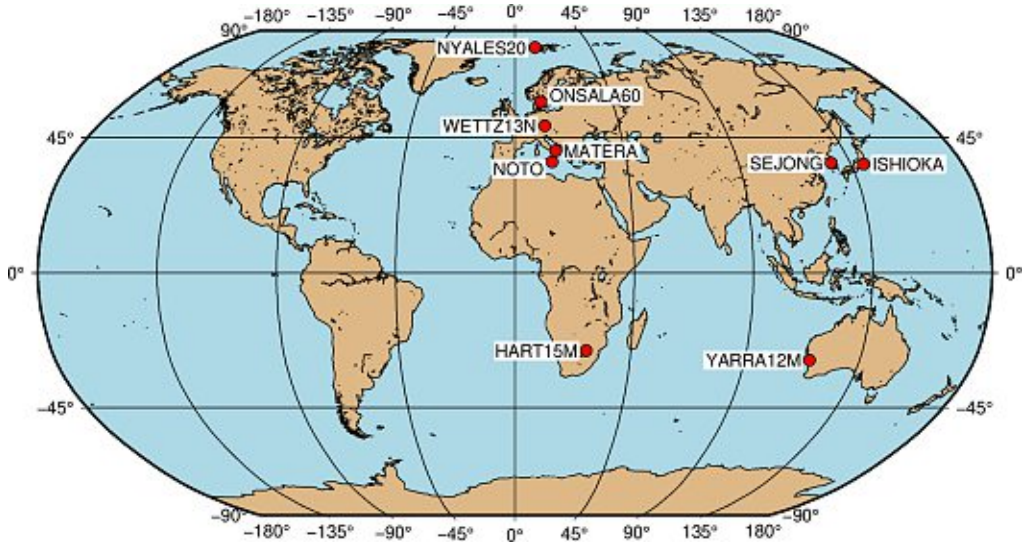

Figure 5.1: VLBI stations participating in the IVS-R1978 session and considered in this study.

5.2. Galileo satellites

Galileo satellites were used as target satellites in this study. A detailed description of the Galileo satellite system can be found in section 2.2. The main characteristics of its constellation are summarized in the following and an overview of the satellites, listed by their position in the orbit (orbital slot), is provided below. There are two more satellites, GSAT0201 and GSAT0202, which are in an elliptical orbit, in so-called extended slots. These are not taken into consideration in the following study.

The Galileo satellite system consists of 24 active satellites in three orbital planes (A, B and C) which are inclined at an angle of 56 degrees to the equator and spaced by 120 degrees to each other. In each orbital plane will be eight satellites separated with an angular distance of 45 degrees and an relative spacing of 15 degrees between the satellites in neighbouring planes. The Galileo constellation has a ground track repeat period of 10 days.

Plane A	**Plane B**	**Plane C**
Slot 1: GSAT0218 – E31	Slot 1: GSAT0220 – E13	Slot 1: GSAT0214 – E05
Slot 2: GSAT0210 – E01	Slot 2: GSAT0221 – E15	Slot 2: GSAT0209 – E09
Slot 3: GSAT0215 – E21	Slot 3: GSAT0204 – E22	Slot 3: GSAT0213 – E04
Slot 4: GSAT0217 – E27	Slot 4: GSAT0219 – E36	Slot 4: GSAT0103 – E19
Slot 5: GSAT0206 – E30	Slot 5: GSAT0101 – E11	Slot 5: GSAT0104 – E20
Slot 6: GSAT0211 – E02	Slot 6: GSAT0102 – E12	Slot 6: GSAT0207 – E07
Slot 7: GSAT0216 – E25	Slot 7: GSAT0222 – E33	Slot 7: GSAT0208 – E08
Slot 8: GSAT0205 – E24	Slot 8: GSAT0203 – E26	Slot 8: GSAT0212 – E03

5.3. Evaluation through visibility

This section gives an overview of the visibility of the Galileo satellites from the defined VLBI network. The visibility is evaluated through the number of stations from which the satellite is observable.

5.3.1. Visibility in percent

The following section analyses the visibility of the Galileo satellites in terms of percentage of time the satellite is visible during the whole session. The visibility is investigated per orbital plane, the satellites ordered by their orbital slots. The interest in a visibility from a high number of stations is the reason that only visibilities from at least four stations simultaneously are considered.

Figure 5.2 shows the percentage of time the satellites in Plane A are observable from at least four stations assuming a cut-off elevation of five degrees. The satellites are ordered by their position in the orbital plane, starting with the satellite in the first slot. The bars indicate the percentage of time the satellite is visible during the whole session, color-coded by the number of stations from which the satellite is observable. In the chart it can be seen, that the satellite GSAT0205 is visible the most and the satellites in the slots ahead of it are becoming with slot to slot less visible until the satellite GSAT0215 in the third slot is least visible. The satellites in the following slots are again from slot to slot more visible.

The visibility of the satellites in Plane B and C shows the same behaviour, as it can be seen in Figure 5.3 and 5.4. In Plane B the satellites GSAT0220 and GSAT0221 and in Plane C the satellites GSAT0208 and GSAT0212 exhibit the lowest visibility. Again the satellites in the following slots are from slot to slot more visible until GSAT0102 in Plane B and GSAT0209 in Plane C reach the highest visibility. The reason for this behaviour is discussed in section 5.3.2.

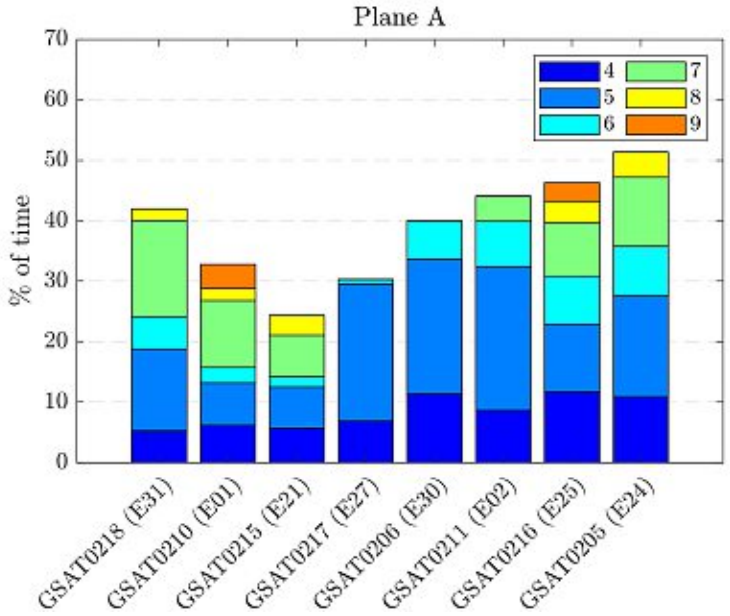

Figure 5.2: Percentage of time the satellites in Plane A, ordered by their slot number, are observable during the 24-hour IVS-R1978 session on December 21, 2020, color-coded by the number of stations from which the satellite is observable. A cut-off elevation angle of five degrees is considered.

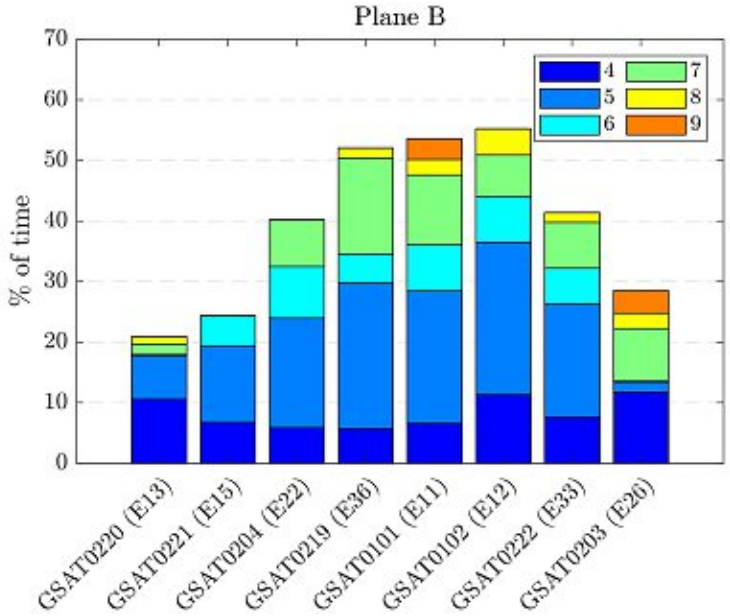

Figure 5.3: Percentage of time the satellites in Plane B, ordered by their slot number, are observable during the 24-hour IVS-R1978 session on December 21, 2020, color-coded by the number of stations from which the satellite is observable. A cut-off elevation angle of five degrees is considered.

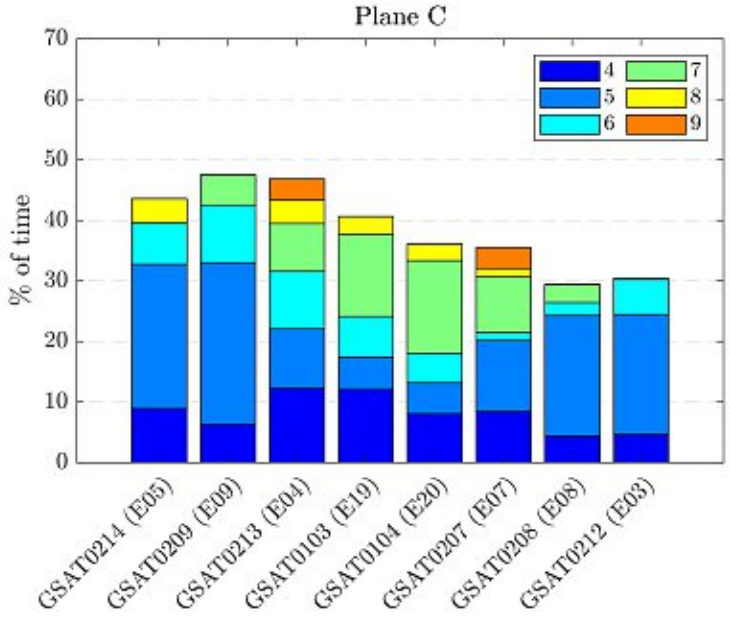

Figure 5.4: Percentage of time the satellites in Plane C, ordered by their slot number, are observable during the 24-hour IVS-R1978 session on December 21, 2020, color-coded by the number of stations from which the satellite is observable. A cut-off elevation angle of five degrees is considered.

5.3.2. Visibility over session time

This section focuses on the visibility of the satellites over the session time. Figure 5.5 shows the visibility over time for the satellites in Plane A, color-coded by the number of stations. It can again be seen, that the satellites GSAT0215 and GSAT0217 are less visible compared to the other satellites in this plane. Further, the chart shows that the visibility of the satellites within this plane is following a pattern that shows that the visibility of two consecutively satellites is similar but time-shifted. The reason for this is the even angular separation of 45 degrees of the satellites within an orbital plane. This causes a shift of the satellite ground tracks in the direction of longitude and therefore a time-shifted visibility can be recognized. The course of the satellite ground track depends on the relative position of the particular satellite and the Earth to each other at that specific time and varies over time, see section 5.3.3.

Figure 5.6 and Figure 5.7 show the visibility over the session time for the satellites in Plane B and C, respectively. The visibility of the satellites in these orbital planes exhibit the same pattern as it is described above.

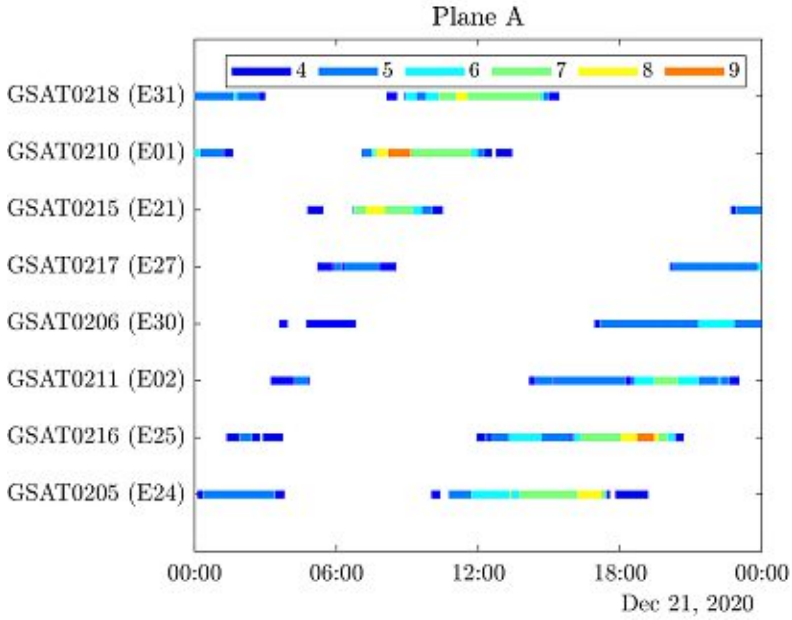

Figure 5.5: Visibility of the satellites in Plane A, ordered by their slot number, during the 24-hour IVS-R1978 session on December 21, 2020 assuming a cut-off elevation angle of five degrees.

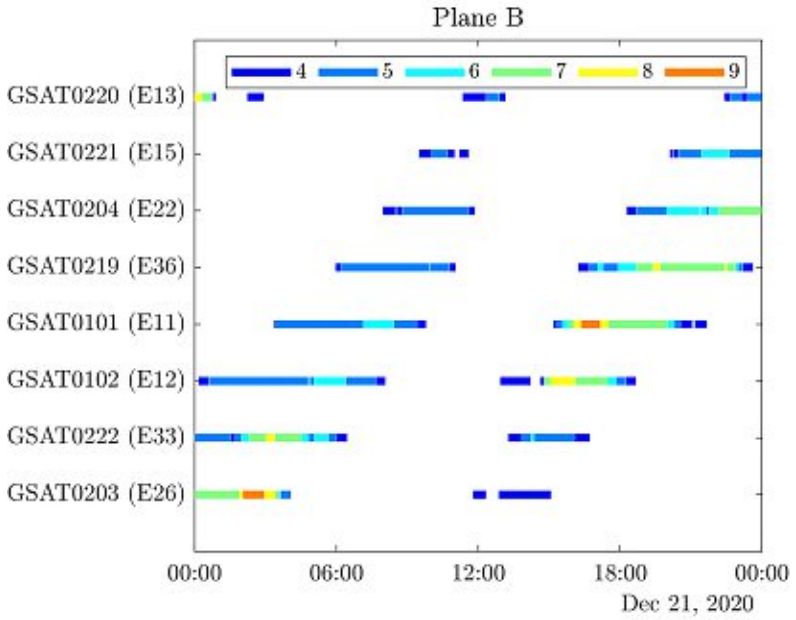

Figure 5.6: Visibility of the satellites in Plane B, ordered by their slot number, during the 24-hour IVS-R1978 session on December 21, 2020 assuming a cut-off elevation angle of five degrees.

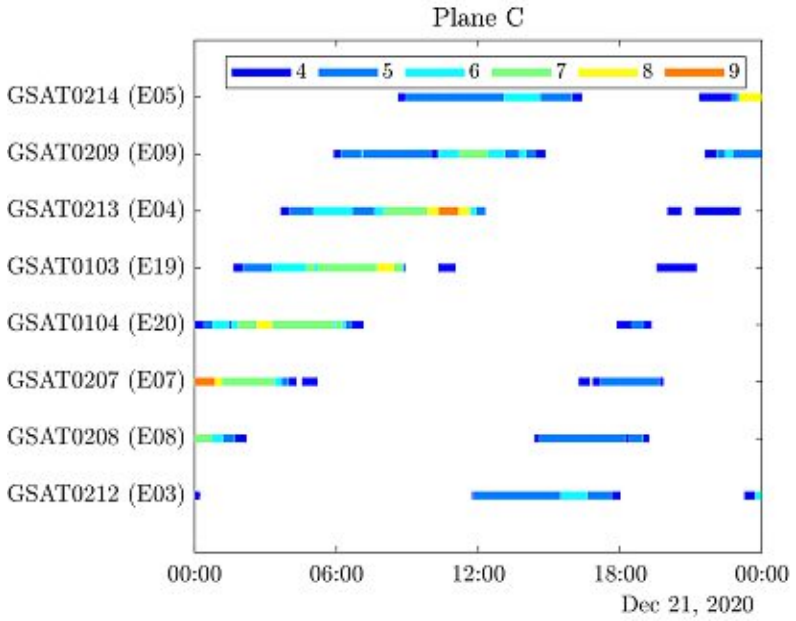

Figure 5.7: Visibility of the satellites in Plane C, ordered by their slot number, during the 24-hour IVS-R1978 session on December 21, 2020 assuming a cut-off elevation angle of five degrees.

5.3.3. Visibility of satellite trajectories

As described in section 5.3.1, the satellites within an orbital plane are visible for a different amount of time during the session. In Plane A the satellites GSAT0205 and GSAT0216 are visible the most for the defined VLBI network. Figure 5.8 and Figure 5.9 depict the ground tracks of these two satellites, color-coded by the number of stations from which the satellites are observable. Based on the course of the track of GSAT0205 it can be seen that the position of the satellite over Earth passes an area, 17 degrees east to 120 degrees east, which is feasible to observe from the VLBI network. The satellite GSAT0216 passes positions over Earth in an area of nine degrees west and 120 degrees east which again results in a high visibility.

The satellites GSAT0215 and GSAT0217 exhibit the smallest visibility from the selected VLBI network. Figure 5.10 depicts the ground track of GSAT02015. During the second half of the session the satellite passes an area over Earth which is only rarely feasible to observe from at least two stations of the defined VLBI network. The same is true for the trajectory of GSAT0217, depicted in Figure 5.11. This results in a lower visibility.

The same insights show the ground tracks of the satellites in Plane B and C which are not further outlined in the following.

This shows that the visibility is strictly related to the course of the trajectory of the satellite and the distribution of the observing antennas. Further, it is important to note that the ground tracks of the satellites are changing over time with a repeat period of ten days. The changes of the visibility over the repeat period of Galileo are analysed in section 5.3.4.

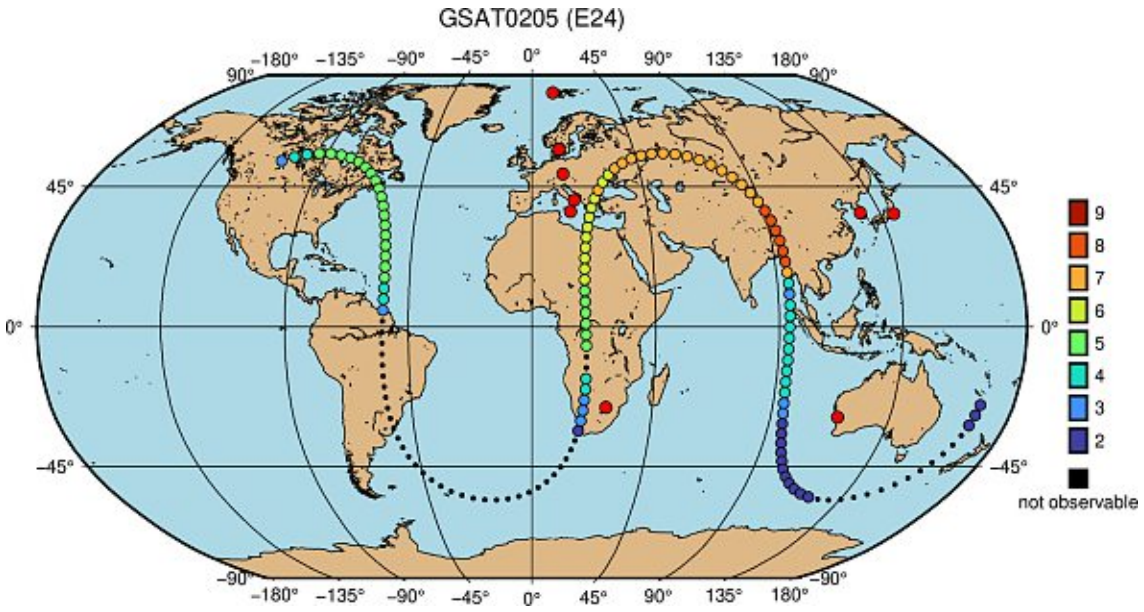

Figure 5.8: Ground track of GSAT0205 (E24) during the 24-hour IVS-R1978 session on December 21, 2020. The dots represent the position of the satellite over Earth in a ten minute interval, color-coded by the number of stations from which the satellite is observable. The smaller black dots represent positions where the satellite is not observable from at least two stations.

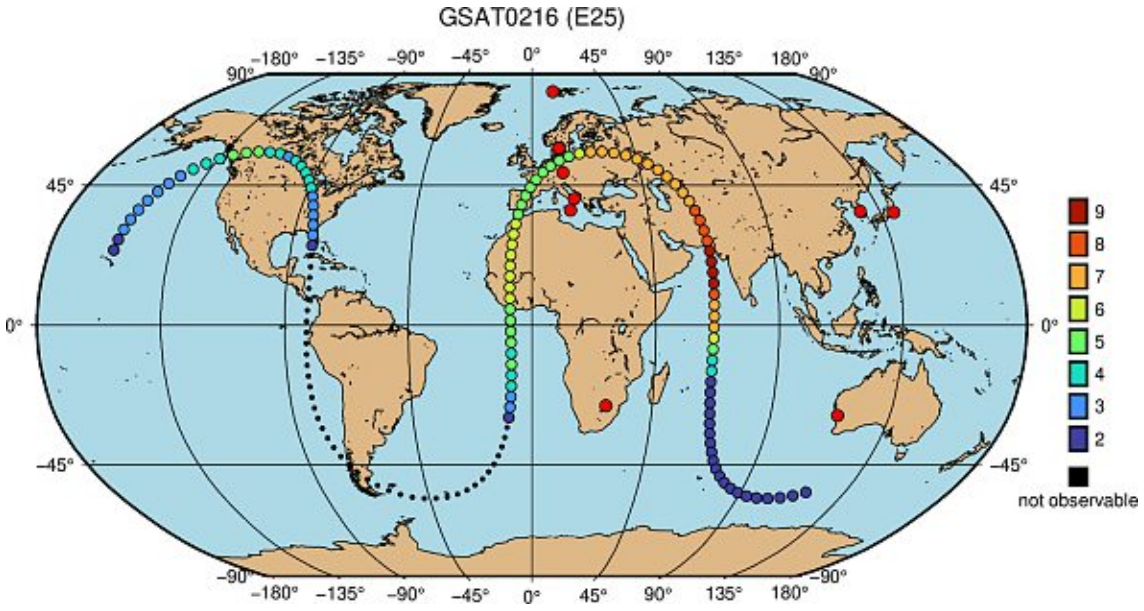

Figure 5.9: Ground track of GSAT0216 (E25) during the 24-hour IVS-R1978 session on December 21, 2020. The dots represent the position of the satellite over Earth in a ten minute interval, color-coded by the number of stations from which the satellite is observable. The smaller black dots represent positions where the satellite is not observable from at least two stations.

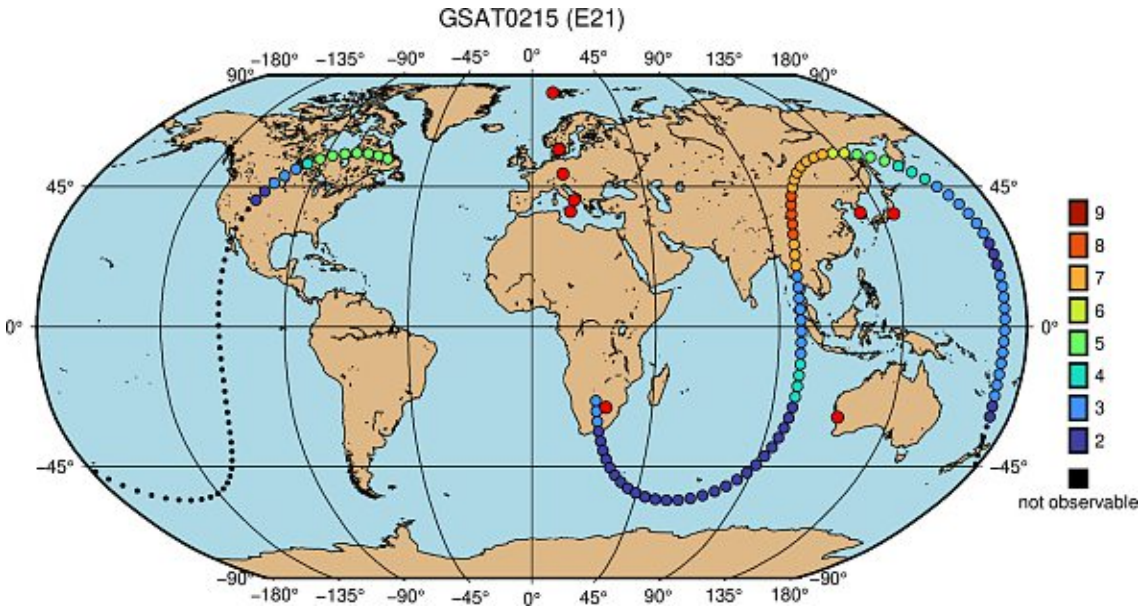

Figure 5.10: Ground track of GSAT0215 (E21) during the 24-hour IVS-R1978 session on December 21, 2020. The dots represent the position of the satellite over Earth in a ten minute interval, color-coded by the number of stations from which the satellite is observable. The smaller black dots represent positions where the satellite is not observable from at least two stations.

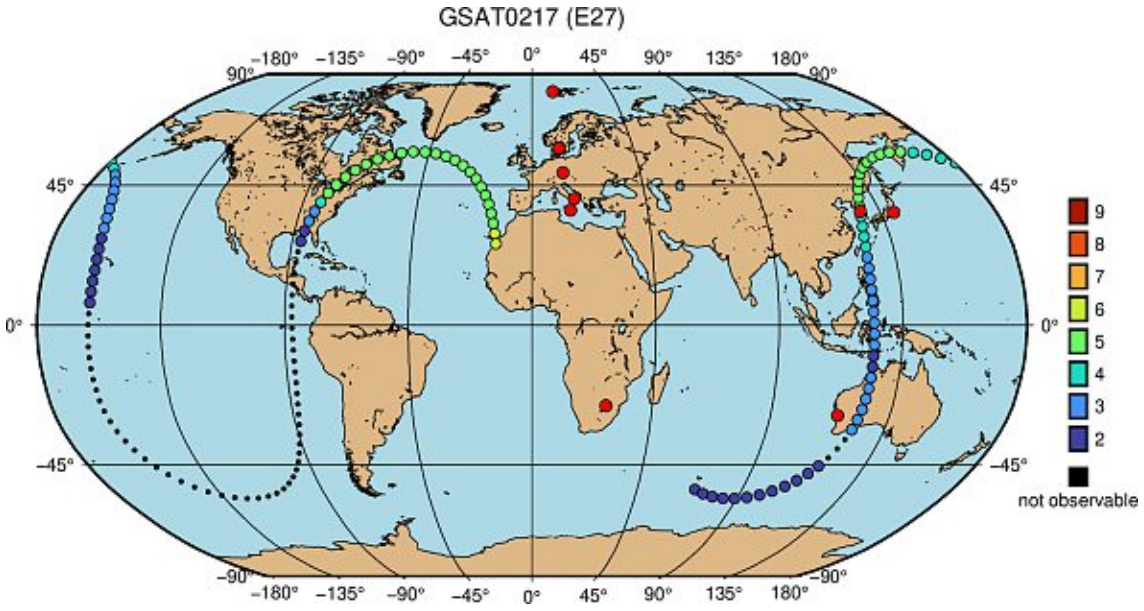

Figure 5.11: Ground track of GSAT0217 (E27) during the 24-hour IVS-R1978 session on December 21, 2020. The dots represent the position of the satellite over Earth in a ten minute interval, color-coded by the number of stations from which the satellite is observable. The smaller black dots represent positions where the satellite is not observable from at least two stations.

5.3.4. Visibility over repeat period of Galileo

The Galileo constellation has a ground track repeat period of ten days. This chapter focuses on the changes concerning the visibility of the Galileo satellites over this time period by the changing relative position of the satellites and the Earth.

The percentage of time the satellites per plane are observable from at least four stations is determined for ten days successively starting with December 21, 2020. Figure 5.12 illustrates the visibility of the Galileo satellites in Plane A over this time period. The bars marked in red represent the satellites which are least visible for each day. It can be seen that the change of the visibility over the days follow a pattern. This can be recognized by looking at the red marked bars in the top view, see Figure 5.12b. The red bars are always shifted two or three slots ahead for consecutively days. This is also true for the other slots meaning that the slot with the satellite which is visible the most on one day is shifted by two or three slots ahead for the following day.

The same insights can be recognized for the satellites in Plane B and Plane C, see Figure 5.13 and 5.14 respectively.

This shows that the visibility of the satellites within a plane is dependent on the relative position of the satellites and the Earth and therefore dependent on the time of the session.

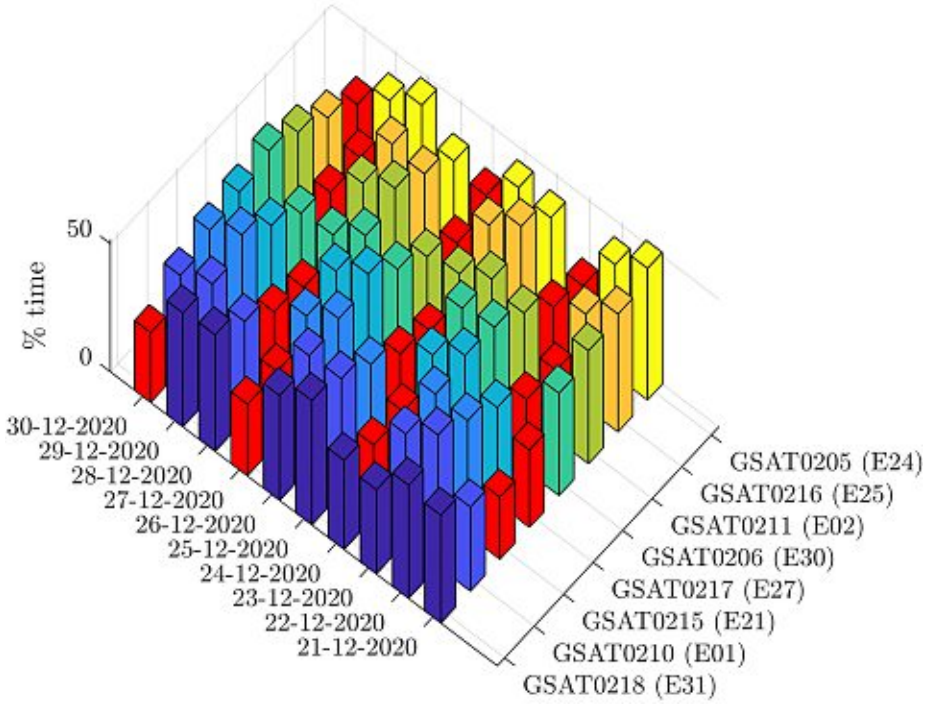

(a) Plane A - 3D view

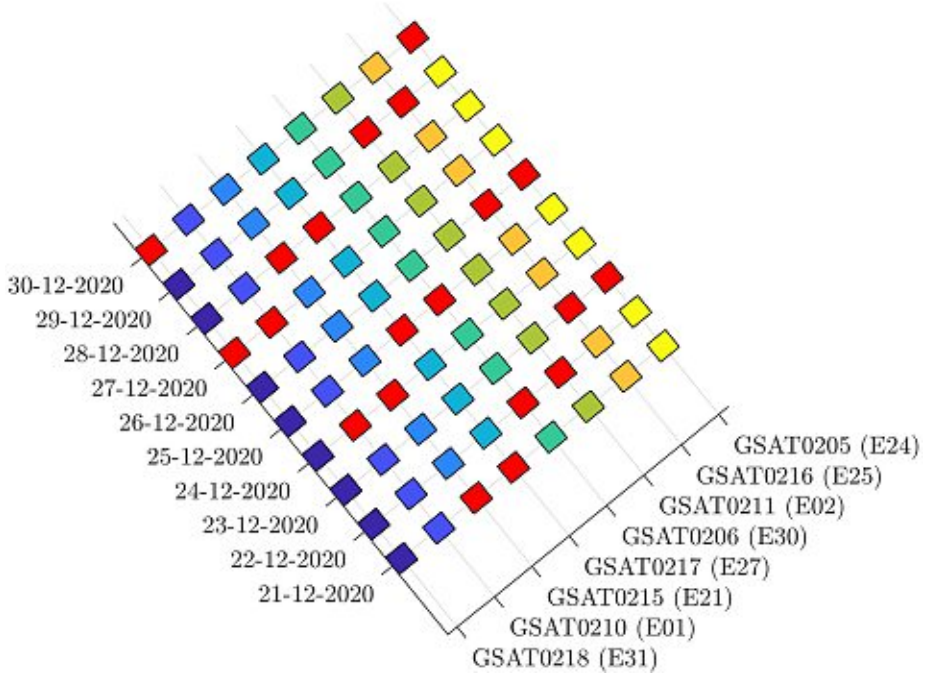

(b) Plane A - top view

Figure 5.12: Percentage of time the satellites in Plane A, ordered by their slot number, are observable from at least four stations over a period of 10 days starting on December 21, 2020. The results are presented in a (a) 3D view and (b) top view where the red marked bars represent the two satellites which are least visible for each day. A cut-off elevation angle of five degrees was considered.

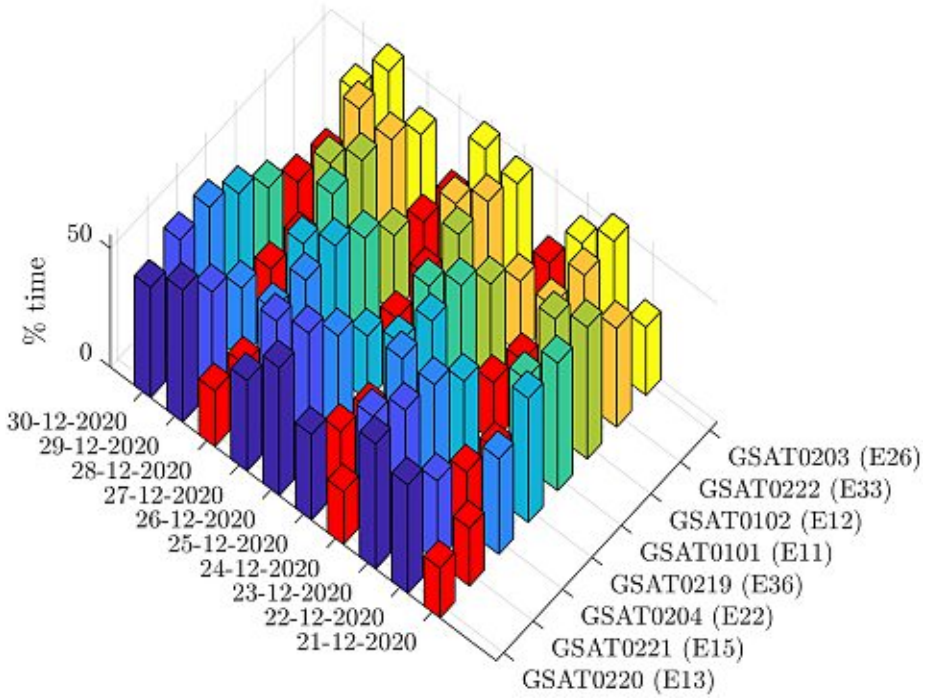

(a) Plane B - 3D view

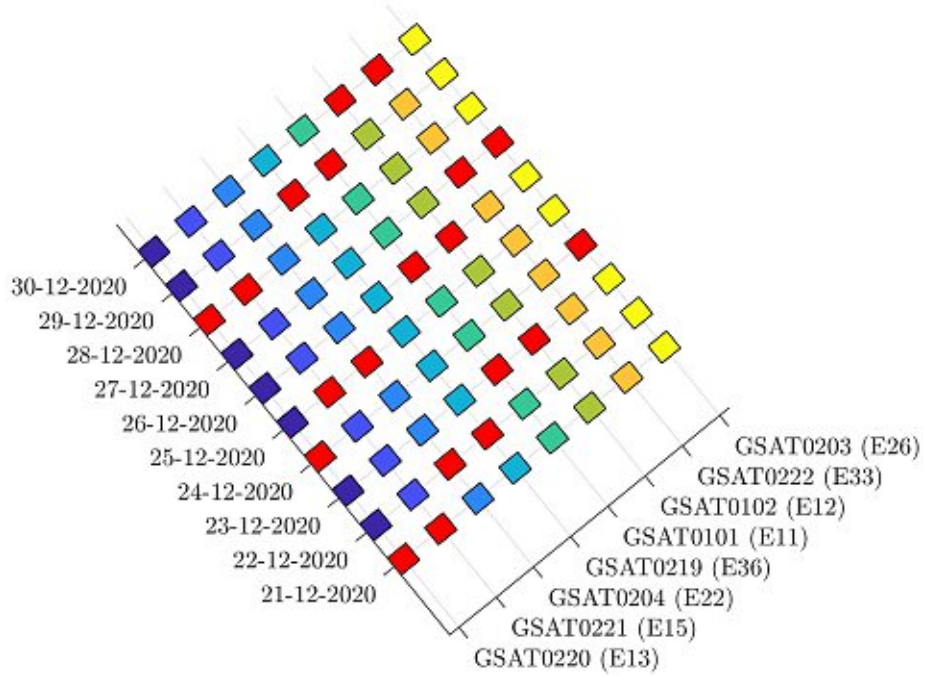

(b) Plane B - top view

Figure 5.13: Percentage of time the satellites in Plane B, ordered by their slot number, are observable from at least four stations over a period of 10 days starting on December 21, 2020. The results are presented in a (a) 3D view and (b) top view where the red marked bars represent the two satellites which are least visible for each day. A cut-off elevation angle of five degrees was considered.

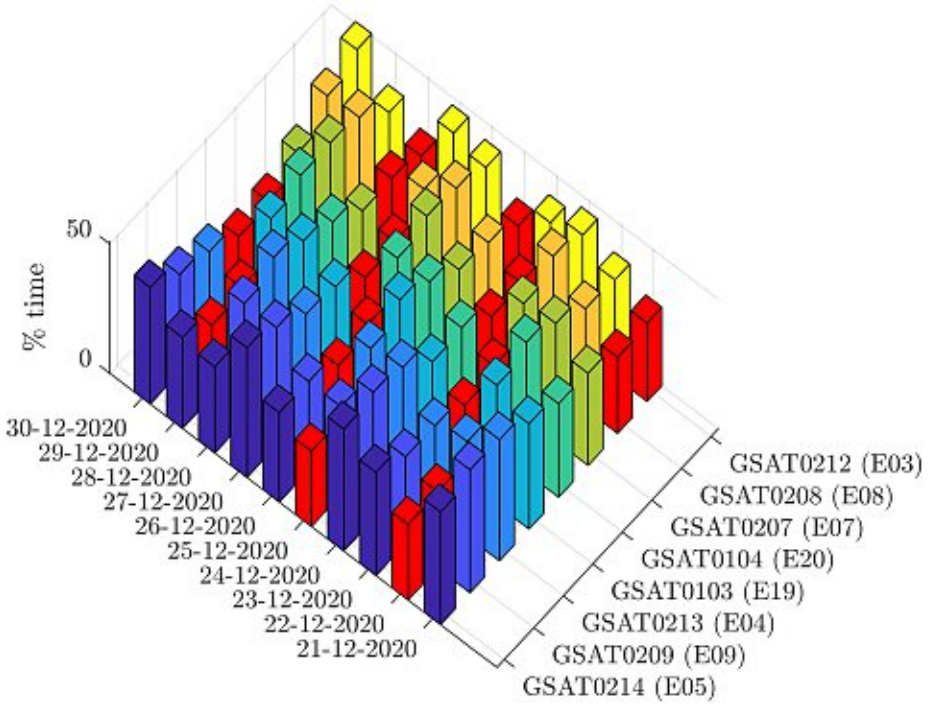

(a) Plane C - 3D view

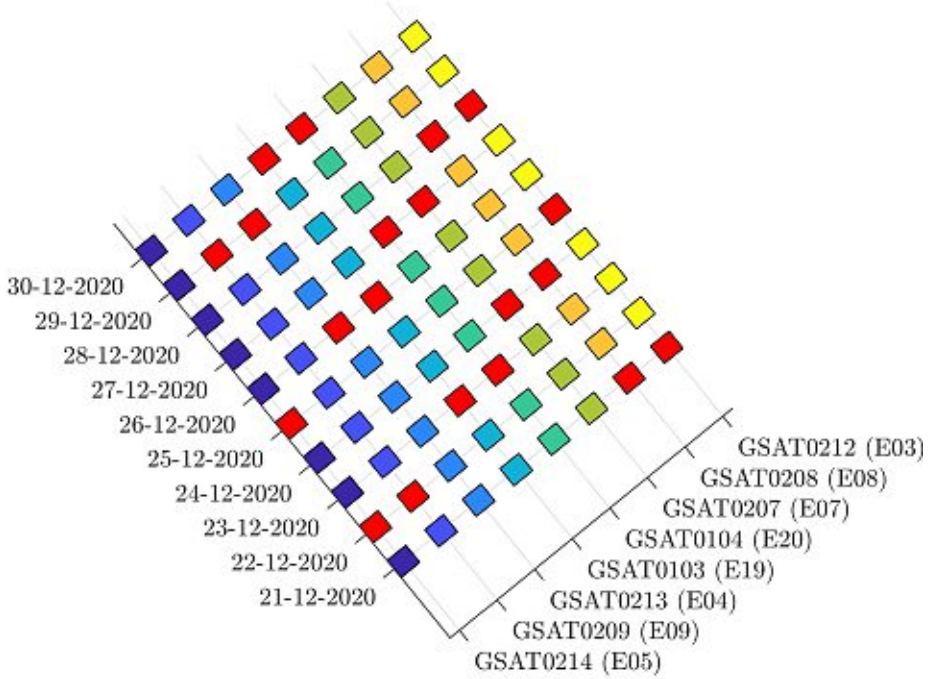

(b) Plane C - top view

Figure 5.14: Percentage of time the satellites in Plane C, ordered by their slot number, are observable from at least four stations over a period of 10 days starting on December 21, 2020. The results are presented in a (a) 3D view and (b) top view where the red marked bars represent the two satellites which are least visible for each day. A cut-off elevation angle of five degrees was considered.

5.4. Evaluation through observation geometry

Observations to satellites with VLBI antennas offer the possibility of determining the absolute orientation, the Right Ascension of the Ascending Node (RAAN), of the satellite constellation directly with respect to ICRF. The precision of the absolute orientation estimated from VLBI observations depends on the observation geometry between the observed baseline and the position of the satellite. In the following, possible satellite observations are evaluated by the observation geometry with using the UT1-UTC Dilution of Precision (UDOP) factor (Belli, 2020).

5.4.1. Estimation of RAAN from VLBI observations

The RAAN of the satellites can be estimated from VLBI observations to satellites using the least squares adjustment. A detailed description of the estimation can be found in Belli (2020).

If a set of antennas observes the same satellite and in total n baselines are observed the linearized observation equations in the Gauß -Markov model can be formulated as

$$\begin{pmatrix} \frac{\delta\Delta\tau_1}{\delta\Omega} \\ \frac{\delta\Delta\tau_2}{\delta\Omega} \\ \vdots \\ \frac{\delta\Delta\tau_\mathrm{n}}{\delta\Omega} \end{pmatrix} \cdot \Omega = A \cdot \Omega = \begin{pmatrix} obs_1 \\ obs_2 \\ \vdots \\ obs_\mathrm{n} \end{pmatrix} \tag{5.1}$$

with $\Delta\tau_\mathrm{i}$ as the observed delay between the reception times of two station observing a satellite and $\frac{\delta\Delta\tau_\mathrm{i}}{\delta\Omega}$ as the partial derivative of the VLBI measurement with respect to the RAAN Ω. A represents the design matrix with each row corresponding to a VLBI observation between two stations, a baseline.

5.4.2. UT1-UTC Dilution of Precision factor

In Belli (2020) the UT1-UTC Dilution of Precision (UDOP) factor was introduced as the sensitivity of VLBI observations to satellites to UT1-UTC caused by the observation geometry.

The lower the UDOP, the better the observation geometry of the satellite to the baseline for determining the orientation of the satellite with respect to ICRF and therefore

the satellite observation is more sensitive to the observation of the RAAN.

The UDOP factor is, as the other Dilution of Precision (DOP) factors used in GNSS, computed from the square root of the trace of the cofactor matrix Q_{xx}.

In the following the mathematical derivation to compute the UDOP factor is described. Equation 5.2 shows the determination of the normal equations matrix N using the design matrix A from equation 5.1. Further, the computation of the cofactor matrix Q_{xx} is outlined in equation 5.3. Finally, the UDOP factor is calculated from the square root of Q_{xx}, see equation 5.4.

$$N = A^{\mathrm{T}}A = \begin{pmatrix} \frac{\delta\Delta\tau_1}{\delta\Omega} & \frac{\delta\Delta\tau_2}{\delta\Omega} & \dots & \frac{\delta\Delta\tau_{\mathrm{n}}}{\delta\Omega} \end{pmatrix} \cdot \begin{pmatrix} \frac{\delta\Delta\tau_1}{\delta\Omega} \\ \frac{\delta\Delta\tau_2}{\delta\Omega} \\ \vdots \\ \frac{\delta\Delta\tau_{\mathrm{n}}}{\delta\Omega} \end{pmatrix} = \left(\frac{\delta\Delta\tau_1}{\delta\Omega}\right)^2 + \left(\frac{\delta\Delta\tau_2}{\delta\Omega}\right)^2 + \dots + \left(\frac{\delta\Delta\tau_{\mathrm{n}}}{\delta\Omega}\right)^2 \tag{5.2}$$

$$Q_{\mathrm{xx}} = N^{-1} = \frac{1}{\left(\frac{\delta\Delta\tau_1}{\delta\Omega}\right)^2 + \left(\frac{\delta\Delta\tau_2}{\delta\Omega}\right)^2 + \dots + \left(\frac{\delta\Delta\tau_{\mathrm{n}}}{\delta\Omega}\right)^2} \tag{5.3}$$

$$UDOP = \sqrt{\frac{1}{\left(\frac{\delta\Delta\tau_1}{\delta\Omega}\right)^2 + \left(\frac{\delta\Delta\tau_2}{\delta\Omega}\right)^2 + \dots + \left(\frac{\delta\Delta\tau_{\mathrm{n}}}{\delta\Omega}\right)^2}} \tag{5.4}$$

In Belli (2020) the mathematical derivation to compute the sensitivity of VLBI observations to satellites to dUT1 (UT1-UTC) is described. The sensitivity of a VLBI observation to a satellite to the Earth-rotation angle and therefore the entry for a row in the design matrix A is represented by formula 5.5.

$$a_{\mathrm{k}} = \vec{e}_3 \cdot \left(\frac{\vec{y}}{R} \times \left(\frac{\vec{R}_1}{\rho_1} - \frac{\vec{R}_2}{\rho_2}\right)\right) \tag{5.5}$$

$\vec{R}_1$ and $\vec{R}_2$ are the position vectors of the two VLBI antennas observing the satellite and $\vec{y}$ is the position vector of the satellite in the Earth-fixed frame. $\rho_{\mathrm{i}} = \|\vec{y} - \vec{R}_{\mathrm{i}}\|$ represents the range from each station to the satellite. By scaling with the Earth radius

R it can be made unit-less. As $\vec{e}_3$ stands for the unit vector in the direction of the third dimension, the entries in the design matrix therefore result in the third component of the cross product.

As the value determined in equation 5.5 is for one baseline between two stations, R_1 and R_2, this is one entry in the design matrix A. Therefore, the UDOP value for an observation of a set of VLBI antennas to a geodetic satellite forming in total n baselines can be written as:

$$UDOP = \frac{1}{\sqrt{{a_1}^2 + {a_2}^2 + \cdots + {a_n}^2}} \tag{5.6}$$

where a_k with $k = 1, 2, ..n$ represent the entries in the design matrix for the n baselines.

5.4.3. Results and analysis of UDOP factor

This section provides results from the computation of the UDOP factor. Again, possible observations with the VLBI network described in section 5.1 to Galileo satellites are determined. Further, the UDOP factor is computed for these possible observations as outlined in equation 5.5, including all baselines between the stations from which the satellite is visible.

In order to investigate the relation between the UDOP factor and the number of stations from which the satellite is visible, Figure 5.15 shows the ground track of the satellite GSAT0102 (E12) color-coded by (a) the number of stations from which it is possible to observe the satellite and (b) the values of the computed UDOP factor. The same is shown for the satellite GSAT0101 (E11) in Figure 5.16.

It can be seen that a high number of stations does not correspond automatically to a low UDOP value. This can be demonstrated on the obtained UDOP factors from satellite GSAT0102 (E12) when it's trajectory is passing over Europe where it is visible for all stations located in Europe. These stations are forming only North-South baselines. Although, the high number of stations from which the satellite could be observed at these positions the obtained UDOP values are rather high. Especially, when the satellite's trajectory is crossing the line described by the baselines between the observing stations the UDOP factor reaches values above five, as this is the worst observation geometry possible for determining UT1-UTC.

The same situation occurs after the satellite travelled southwards and it's trajectory is above South Africa. After crossing Europe and continuing travelling in its orbit the stations in Europe loose the line of sight to the satellite. When the satellite is above

South Africa, it is only visible from stations forming baselines from North to South namely NOTO, MATERA and HART15M. When the satellite is coming closer to cross the extended line between these stations the UDOP factor again reaches high values above five.

The best observation geometry occurs when the satellite passes through two stations forming a baseline from East to West. This situation arises for GSAT0102 (E12) when it's trajectory passes between the station located in South Africa and the station located in Australia. Although, it is only visible for these two stations the UDOP values are low which corresponds to a high sensitivity to UT1-UTC.

When the satellite continues travelling in its orbit a jump in the UDOP value from below 0.5 to a value between two and three can be recognized. This can again be explained by the changing observation geometry. At the positions before the jump of the UDOP value, the satellite is visible for four stations simultaneously, see Figure 5.15a. By travelling further the station in South Africa is not longer able to observe it and the number of stations from which it is visible drops for a short period of time to three, namely the stations in Asia, SEJONG and ISHIOKA and the station in Australia YARRA12M. These stations again form baselines from North to South which correspond to an observation geometry with a low sensitivity to UT1-UTC and high values for the UDOP factor. When the satellite moves further in its orbit it again becomes visible for the stations in Europe. Therefore, baselines from East to West are formed which results in low values for the UDOP factor.

This shows that the obtained UDOP value does not correspond to the number of stations from which the satellite is visible but it depends on the geometry between the observing stations and the position of the satellite.

Figure 5.16 shows the results from the computation of the UDOP factor for GSAT0101 (E11). In this Figure the same findings as explained above can be recognized.

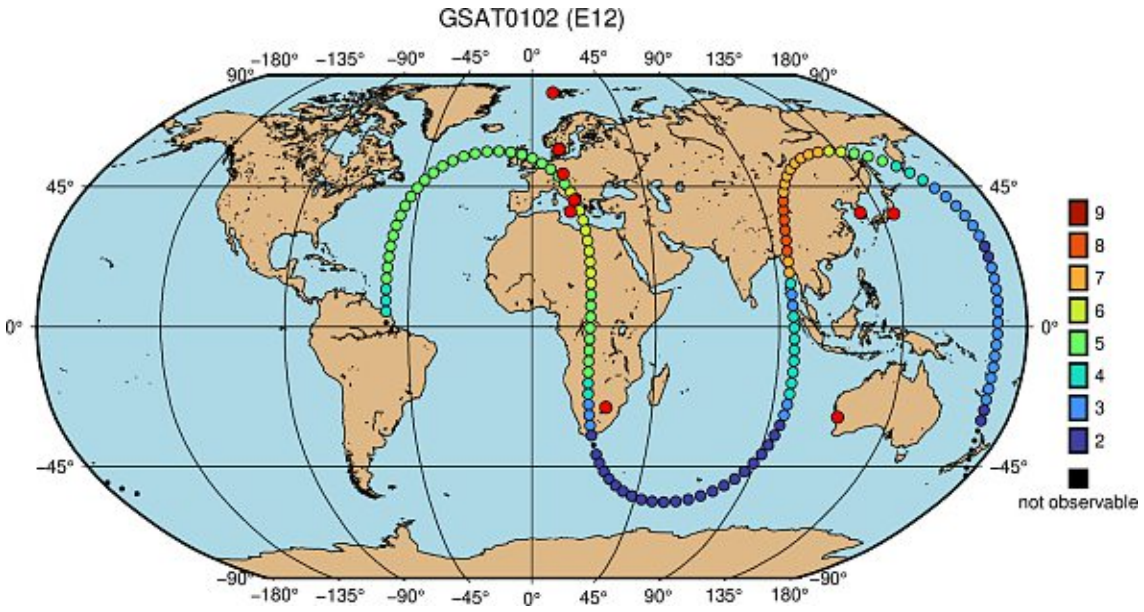

(a) number of stations

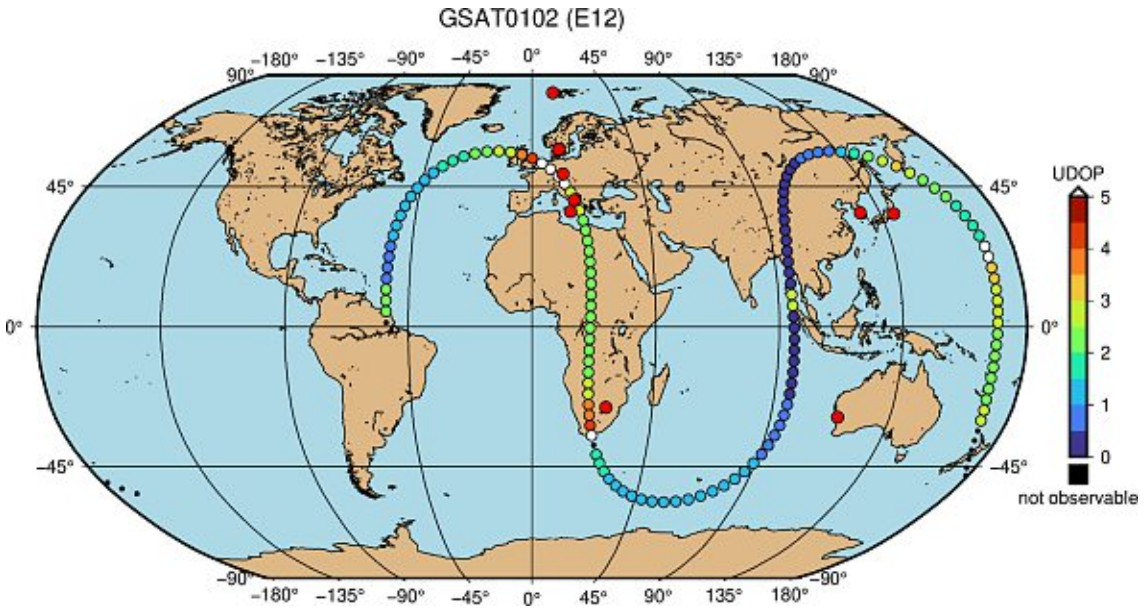

(b) UDOP factor

Figure 5.15: Ground track of GSAT0102 (E12) during the 24-hour IVS-R1978 session on December 21, 2020. The dots represent the position of the satellite over Earth in a ten minute interval color-coded by (a) number of stations from which the satellite is visible and (b) values of the UDOP factor. The smaller black dots represent positions where the satellite is not visible from at least two stations.

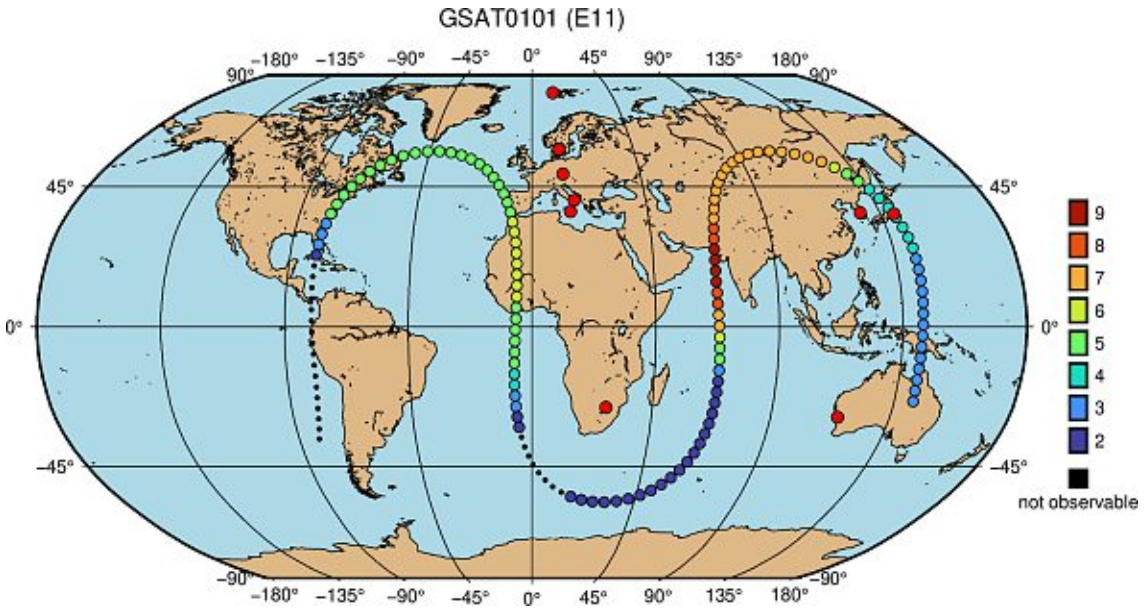

(a) number of stations

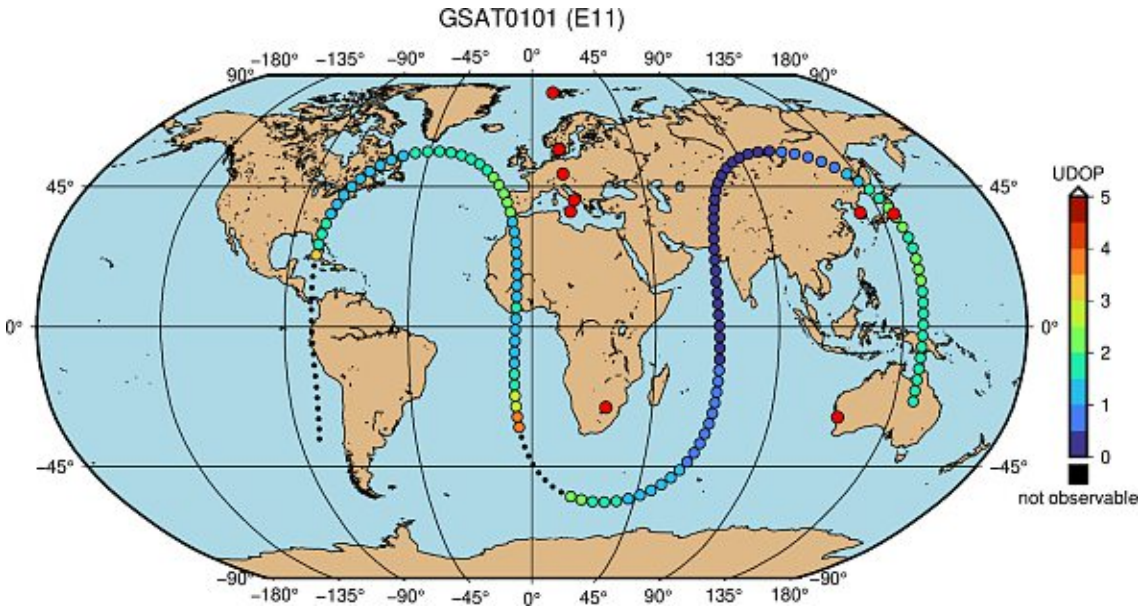

(b) UDOP factor

Figure 5.16: Ground track of GSAT0101 (E11) during the 24-hour IVS-R1978 session on December 21, 2020. The dots represent the position of the satellite over Earth in a ten minute interval color-coded by (a) number of stations from which the satellite is visible and (b) values of the UDOP factor. The smaller black dots represent positions where the satellite is not visible from at least two stations.

5.5. Discussion of results

5.5.1. One satellite equipped with VLBI transmitter

The study of the visibility of the Galileo satellites showed that there are no differences of the visibility between the three orbital planes and between the satellites within the orbital planes. The visibility of a satellite and the geometry between the observed baselines and the satellite's position depends on the distribution of the observing station network and on the session time, as the trajectory of the satellite is changing over the repeat period of Galileo. Therefore, if there is one satellite of the Galileo constellation equipped with a VLBI transmitter, none of the orbital planes and none of the slots within the orbital planes is preferable for placing this satellite, they are all equivalent.

5.5.2. Two satellites equipped with VLBI transmitter

If there are in total two satellites of the Galileo constellation equipped with a VLBI transmitter, there are different possibilities for their placing in the orbital planes. Both satellites can be in the same plane or they can be in different planes. In the following these two scenarios are discussed.

Two satellites in the same orbital plane

If the two satellites equipped with a VLBI transmitter are in the same plane, there are still different possibilities regarding their angular distance. These two satellites can be in consecutive slots which means that they are separated with an angular distance of 45 degrees but they can also be in any other combination of different slots. Figure 5.19 shows all possible scenarios how the two satellites can be separated within Plane A.

If the satellites are in consecutive slots, see Figure 5.19a, it can be seen that the ground tracks of the satellites are similar and only shifted a little in the direction of longitude. Due to the similar trajectory the observation geometry between any defined VLBI network and the two satellites is similar as well. Therefore, there are observations to two different satellites available but the observation geometry between them and the observing network is similar. This can be a disadvantage if the observation geometry between the selected network and both satellites is not that suitable for determining UT1-UTC.

Figure 5.17 shows the visibility of the two satellites over the session time of IVS-R1978 from the network defined in section 5.1. It can be seen that the time periods during which both satellites are visible are mostly overlapping. As the ground tracks of the

satellites cover the same range of longitudes, both satellites are visible for similar time periods from the defined VLBI network but there are also time periods where none of both satellites is visible. This can be a problem for short sessions taking place during the period where both satellites aren't visible. This combination therefore does not provide the visibility of at least one satellite over the whole time of the session.

Figure 5.19d illustrates the situation if the two satellites are separated with the biggest possible angular distance, a distance of 180 degrees which corresponds to satellites in slots with three slots in between. Further, due to the bigger shift of the trajectories of the satellites the observation geometry between a defined VLBI network and the satellites is different. This allows to choose the observation to the satellite with the better observation geometry during the scheduling process.

The wide angular distance between the satellites results in different time periods during which the satellites are observable from VLBI network defined in section 5.1, see Figure 5.18. As the course of the ground tracks differs and covers different ranges of longitudes the time periods during which the satellites are visible are less overlapping and therefore at least one satellite is visible during the whole session.

The same is true for two satellites equipped with a VLBI transmitter within Plane B and Plane C. The results are not further listed here.

The results of this analysis show that, if two satellites within the same plane are equipped with a VLBI transmitter, it would be better to equip satellites which are widest apart from each other. This results in the coverage of an in total bigger range of longitudes and in different observation geometries between any defined VLBI network and the satellite positions.

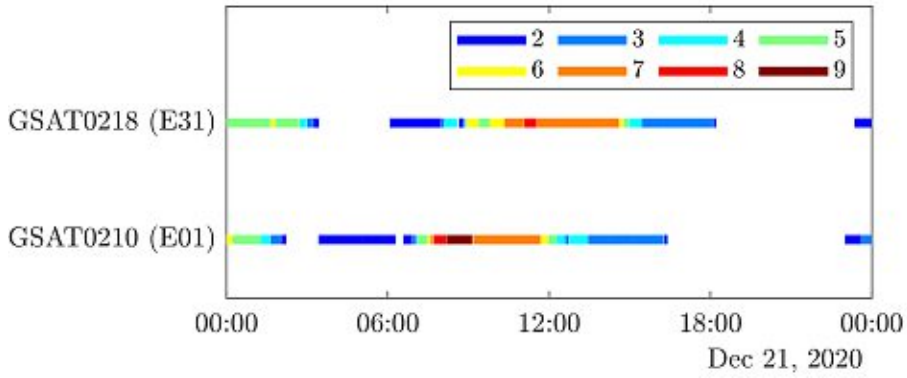

Figure 5.17: Visibility of two satellites in consecutive slots in Plane A, over the 24-hour IVS-R1978 session on December 21, 2020 assuming a cut-off elevation angle of five degrees.

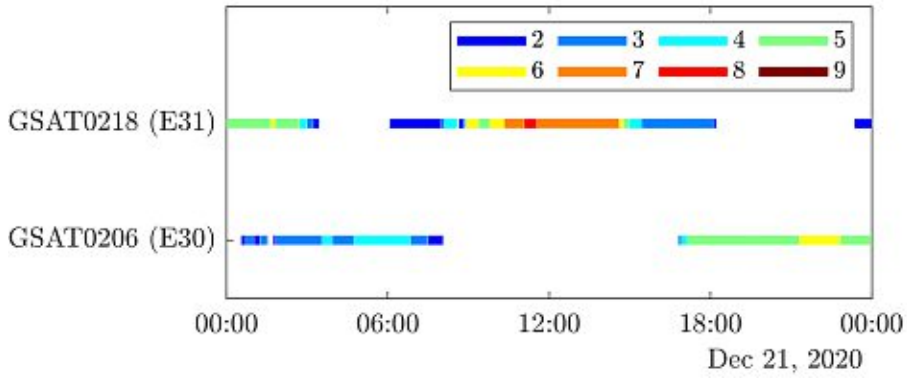

Figure 5.18: Visibility of two satellites in slots with the greatest angular distance in Plane A, over the 24-hour IVS-R1978 session on December 21, 2020 assuming a cut-off elevation angle of five degrees.

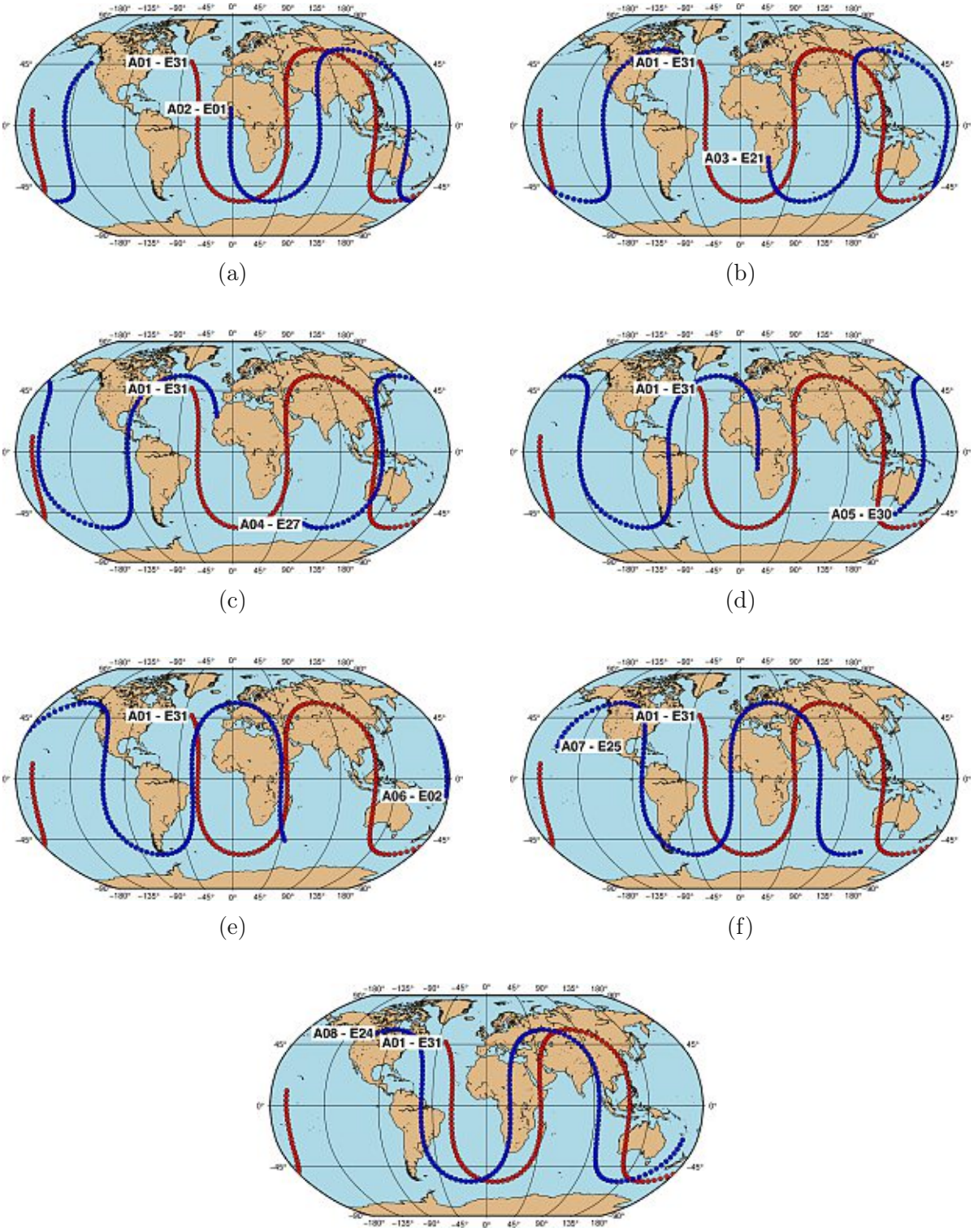

Figure 5.19: Ground tracks of two satellites within Plane A with different angular separations of (a) 45 degrees, (b) 90 degrees, (c) 135 degrees, (d) 180 degrees, (e) 225 degrees, (f) 270 degrees and (g) 315 degrees over the 24-hour session on December 21, 2020.

Two satellites in different orbital planes

The following section discusses the different possibilities which arise when the two satellites equipped with a VLBI transmitter are placed in different orbital planes. There are in total three main combinations for two satellites in different orbital planes, one per Plane A and B, one per Plane B and C, and one per Plane C and A. These combinations again provide different possibilities in terms of the position of the satellites within the planes.

The orbital planes are spaced by 120 degrees to each other and the satellites in neighbouring planes in equivalent or adjacent slots, depending on the planes, differ by 15 degrees in terms of true anomaly, which represents the angle between the direction of perigee and the direction of the satellite. This means that if a satellite in Plane A passes the perigee the satellite in the same slot in Plane B has a true anomaly of 15 degrees meaning that the satellite's orbital position is already 15 degrees ahead of the position of the perigee.

The configuration of the satellites in the three orbital planes is illustrated in Figure 2.4. As already mentioned, the orbital planes are all spaced by 120 degrees to each other and the relative spacing between the satellites depends on the adjacent planes.

More specifically, the relative spacing between a slot in Plane A to the equivalent slot in Plane B is 15 degrees, meaning that for instance the first slot in Plane A and the first slot in Plane B differ by 15 degrees in terms of true anomaly.

The same is true for the satellites in Planes B and C, the relative spacing between a slot in Plane B and the equivalent slot in Plane C is 15 degrees.

For Plane C and A the situation concerning the relative spacing between the slots is different. In this case a relative spacing of 15 degrees occurs between a slot in Plane C and a slot in Plane A which is one orbital position ahead, for instance the first slot in Plane C and the second slot in Plane A differ by 15 degrees in terms of true anomaly.

Figure 5.20 illustrates the scenario of one equipped satellite in Plane A and one in Plane B. In order to investigate the different relative positions between the satellites in Plane A and B, one satellite corresponds always to the satellite in the first slot in Plane A and the second satellite changes over all eight slots in Plane B. The characteristics discussed above, a differing geometry of the two satellites and a differing coverage of longitudes, are met best from the combination with the satellite in slot eight of Plane B, see Figure 5.20h. This means that with one satellite per Plane A and one satellite per Plane B the best combination arises when there are six slots in between the two equipped satellites.

In other words, placing one of the equipped satellites in Plane A the best combination is met by placing the second satellite in Plane B one slot behind the slot of the satellite in Plane A. Another example of a possible combination would be to place the satellite in Plane A in the second slot and the satellite in Plane B in the first slot.

The same scenario is shown for one satellite per Plane B and C in Figure 5.21. It can be recognized that the relative positions of the ground tracks of the satellites in Plane B and C are similar to those of the satellites in Plane A and B concerning the offset in terms of longitude. Apart from the different courses of the tracks the relative position to each other is similar which can be seen by comparing with Figure 5.20. This is because the relative spacing between satellites in Plane A and B is the same for satellites in Plane B and C, meaning that equivalent slots are spaced by 15 degrees in terms of true anomaly. Therefore, again the combination with six slots between the equipped satellites, counting upwards, is the best combination, see Figure 5.21h.

As described above, the relative spacing between the slots in Plane C and A are different meaning that a relative spacing of 15 degrees occurs between a slot in Plane C and one slot ahead in Plane A, for instance the first slot in Plane C and the second slot in Plane A. Figure 5.22 shows the analysis for one of the equipped satellites in Plane C and the other one in Plane A. In order to maintain consistency to the scenarios described above, one satellite always corresponds to the satellite in the first slot of Plane C and the second satellite changes over all eight slots in Plane A but this time starting with the satellite in the second slot. Therefore, again similarities concerning the offset in terms of longitude can be seen compared to the situations of placing the equipped satellites in Plane A and B or in Plane B and C. Figure 5.22h shows again the best combination of placing the satellites in Plane C and A but this time this configuration corresponds to satellites in equivalent slots due to the different situation of the relative spacing. This means placing one of the equipped satellites in Plane C the best combination arises by placing the second satellite in Plane A in the same slot which is in terms of true anomaly behind the slot of the satellite in Plane C.

If the found insights are studied with regard to Figure 2.4 it can be seen that placing the satellites in Plane A and B or Plane B and C with six slots in between (counting upwards) or in Plane C and A in equivalent slots always corresponds to a similar relative position between the two equipped satellites.

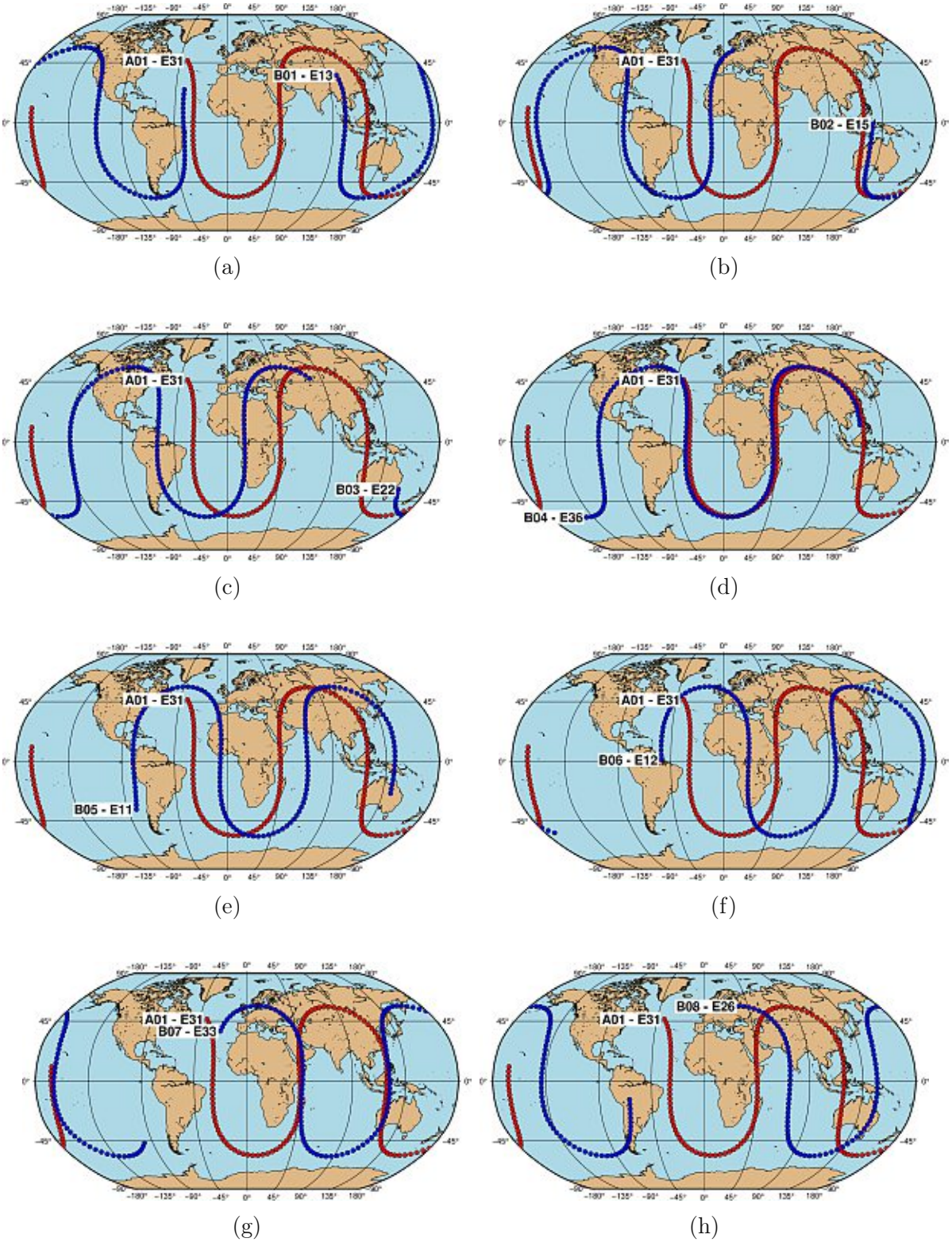

Figure 5.20: Ground tracks of one satellite in Plane A and one in Plane B in different relative positions to each other. The satellite in Plane A always corresponds to the satellite in slot 1 and the satellite in Plane B corresponds to the satellite in (a) slot 1, (b) slot 2, (c) slot 3, (d) slot 4, (e) slot 5, (f) slot 6, (g) slot 7 and (h) slot 8.

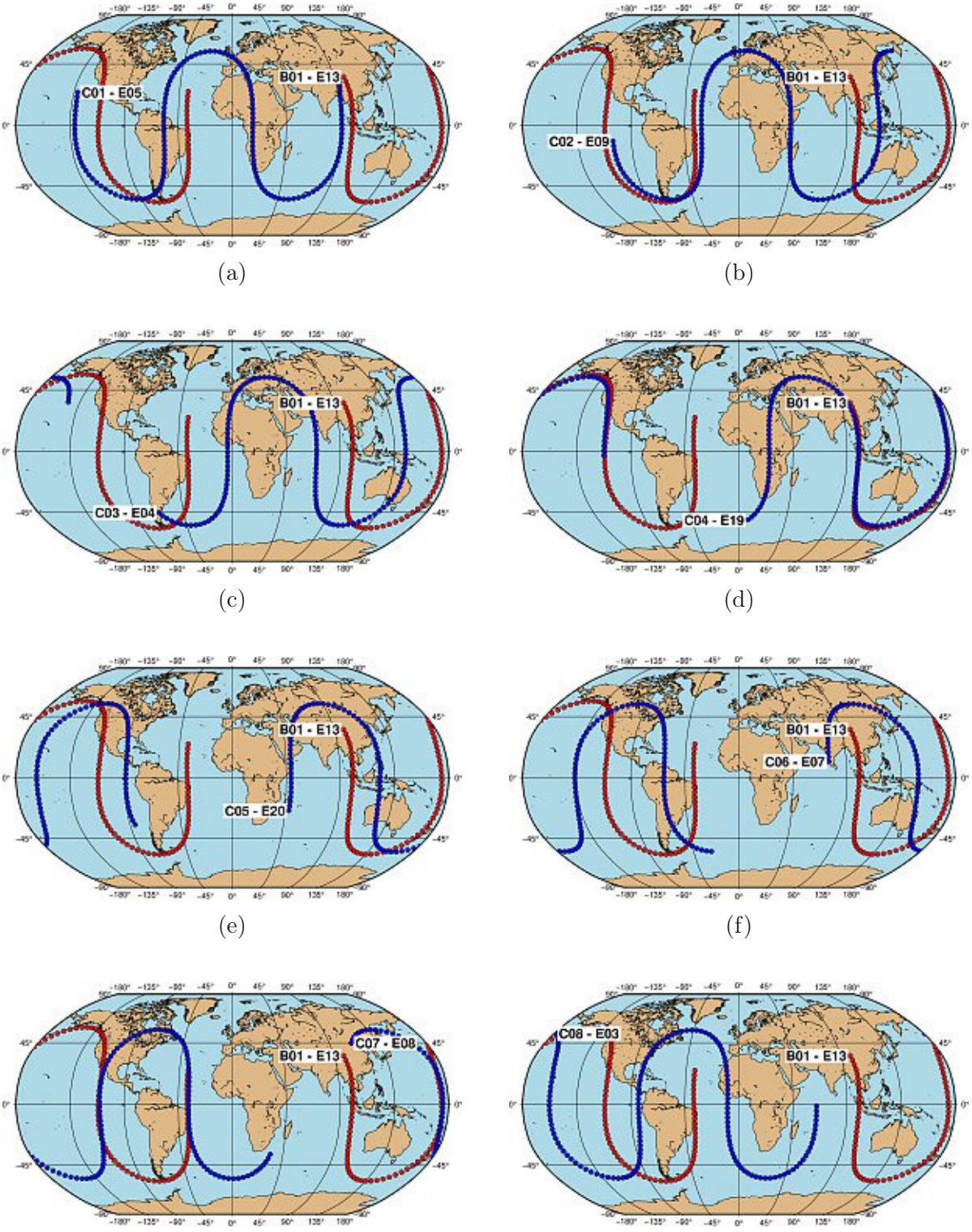

Figure 5.21: Ground tracks of one satellite in Plane B and one in Plane C in different relative positions to each other. The satellite in Plane B always corresponds to the satellite in slot 1 and the satellite in Plane C corresponds to the satellite in (a) slot 1, (b) slot 2, (c) slot 3, (d) slot 4, (e) slot 5, (f) slot 6, (g) slot 7 and (h) slot 8.

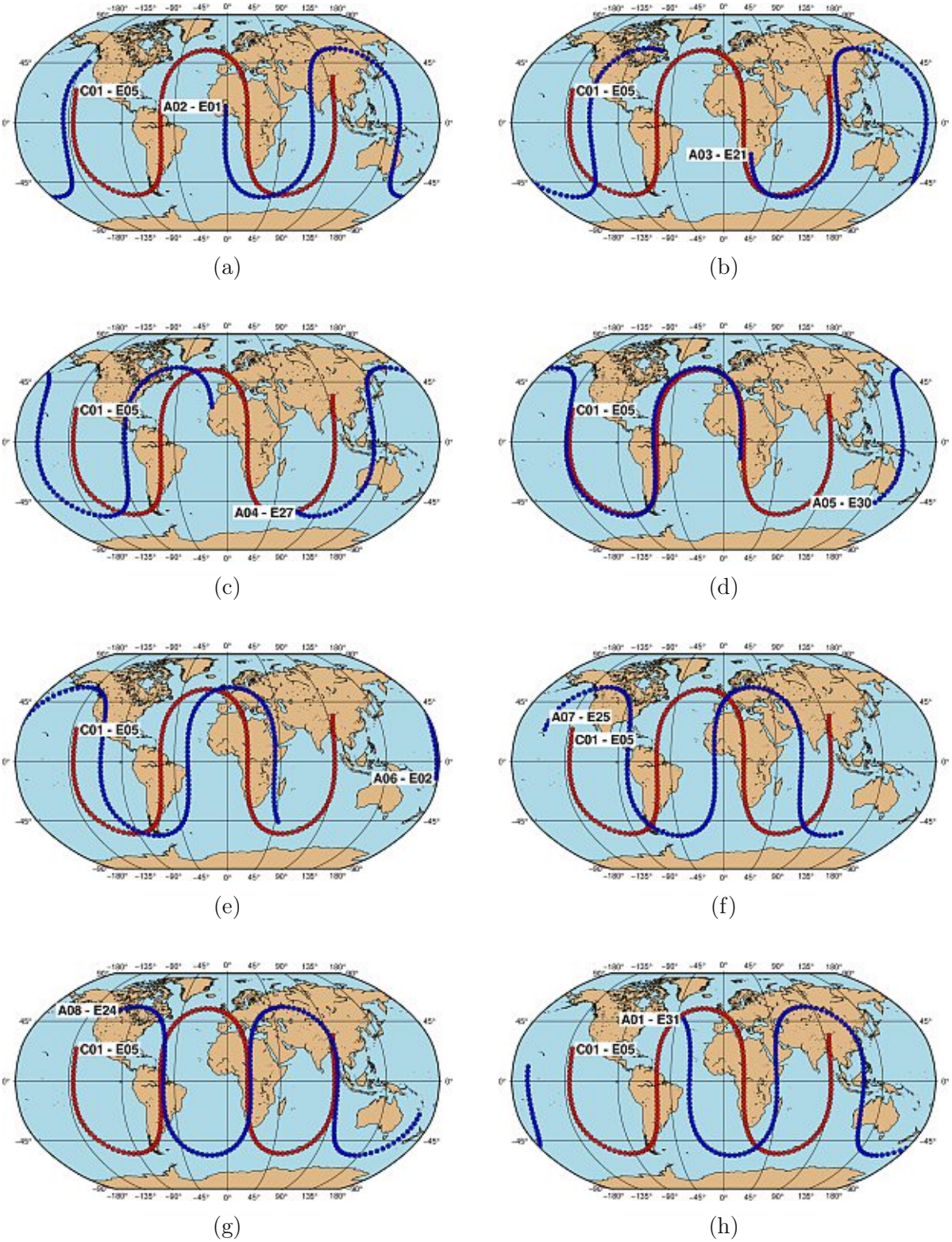

Figure 5.22: Ground tracks of one satellite in Plane C and one in Plane A in different relative positions to each other. The satellite in Plane C always corresponds to the satellite in slot 1 and the satellite in Plane A corresponds to the satellite in (a) slot 2, (b) slot 3, (c) slot 4, (d) slot 5, (e) slot 6, (f) slot 7, (g) slot 8 and (h) slot 1.

6. Summary and Conclusion

The satellite scheduling module in VieSched++ provides a user friendly tool to include observations to satellites in a schedule. It determines the position of the satellite by propagating the corresponding TLE dataset using the SGP4 model. The advantage of using TLE data for the orbit prediction is its wide availability for Earth satellites. Further, it checks if the satellite is visible from at least two of the selected stations and if the required conditions, such as Sun distance and antenna slew rates, are fulfilled in order to allow a feasible satellite observation. There are two different possibilities for scheduling observations to satellites, the semi-manual and the automatic approach.

Scheduling satellite observations with the semi-manual approach allows the user to investigate the different satellites in terms of its visibility and elevation angles over time at which the satellites are visible from the defined VLBI network. The user can manually select and adjust the possible satellite scans through the GUI of VieSched++. These scans are added as a-priori scans to the schedule and in a second phase the remaining part of the schedule will be filled with observations to quasars using the recursive scan selection algorithm. The scheduler therefore has full control over the selected satellite scans and can select ideal satellite scans. The disadvantage is that the process requires experience and is time-consuming.

The scheduling of satellite observations in the automatic fashion allows the generation of a schedule with observations to quasars and satellites in one step without interaction from the user. The satellite is treated as a quasar and the schedule is generated scan by scan using the general algorithm of VieSched++. The benefit is the rather fast generation of a schedule including satellite scans compared to the semi-manual approach but the downside is the limited control about the selected satellite observations.

The combination of quasar and satellite observations in one schedule provide the opportunity to use the quasar observations as calibration sources. The observations to satellites equipped with a VLBI transmitter offer new possibilities such as the direct determination of the absolute orientation of the satellite orbit with respect to the ICRF. Further, these kind of observations allow the tying of space-geodetic techniques with high precision and have therefore implications on the ITRF.

The conducted evaluation study of observations to Galileo satellites with a VLBI network showed that the Galileo satellites exhibit a high visibility for an IVS-R1 network. The satellite which is visible least still shows a visibility for 20% of the session time and

therefore can be observed several times during a 24-hour session. Further, the study showed that for determining the absolute orientation of a satellite orbit it is not important to observe the satellite with a high number of stations simultaneously but it is rather important to achieve a suitable observation geometry between the observing stations and the position of the observed satellite.

There are no differences between the different orbital planes and between the slots within the orbital planes in terms of their visibility. If one satellite would be equipped with a VLBI transmitter there is therefore none of the orbital planes and none of the orbital slots preferable.

The study of two satellites equipped with a VLBI transmitter within the same plane revealed that the satellites should be widest apart from each other as this provides different relative positions between the Earth and the satellites and therefore different observation geometries between any defined VLBI network and the trajectories of the satellites occur from which the scheduler can choose.

The scenario of two satellites equipped with a VLBI transmitter in different planes showed that the different possibilities in which of the planes the satellites are placed are similar to each other.

If the satellites are placed in Plane A and B, the best combination arises when there are six slots between the slot of the satellite in Plane A and the slot of the satellite in Plane B, counting upwards such as the satellite in Plane A placed in the first slot and the satellite in Plane B in the eighth slot, giving six slots in between. The same is true for placing the satellites in Plane B and C.

The analysis of the two satellites equipped with a VLBI transmitter placed in Plane C and in Plane A showed that the best combination is met when placing them in equivalent slots. This is due to the different situation of the relative spacing between the slots Plane C and A but presents the same relative constellation between the two equipped satellites as it does by placing the satellites in the Plane A and B or Plane B and C with six slots in between.

To conclude, a VLBI transmitter on one or more satellites of the next generation of Galileo would definitely help to achieve goals like the tying of space-geodetic techniques but also to directly determine the absolute orientation of the satellite orbit with respect to ICRF. The newly developed possibility to schedule observations to satellites with the software VieSched++ certainly provides a step towards research activities in the field of VLBI observations to satellites.

Further improvement is being considered in the selection of the satellite observations. Especially, the automatic selection of the satellite observations can be improved by introducing a metric which allows their evaluation. A possible metric could be the UDOP factor as this factor is an indicator for the sensitivity of the observation geometry for determining the orientation of the satellite with respect to ICRF. During the automatic scheduling process the software could select the possible satellite scans which exhibit the lower UDOP factor.

A. Coordinate systems

A.1. Earth-Centered Inertial System

The Earth-Centered Intertial coordinate frame is useful to describe the position and motion of celestial bodies and satellites. It has its origin at the center of the Earth and it is fixed in space relative to the stars and therefore not rotating. It is defined as a cartesian coordinate system with the coordinates of an object as the distance from the origin along the three orthogonal axes. The z-axis points in the direction of the Earth's rotational axis, the x-axis points in the direction of the vernal equinox which is the point where the Earth's equatorial plane and the ecliptic plane, the plane of the Earth's orbit around the Sun, are intersecting. The y-axis completes the system to a right-handed orthogonal system. Figure A.1 illustrates an ECI system.

The TLE element sets are propagated with the SGP4 model which results in a position and velocity vector of the satellite in the ECI system. In particular, the resulting ECI position and velocity vector correspond to a ECI frame relative to the "true equator and mean equinox of the epoch" of the TLE element set, the so-called ECI TEME system.

This specification is necessary as the direction of the Earth's rotational axis and the direction of the vernal equinox are wandering slowly over time. The observations of satellites are made by stations located and therefore fixed to the Earth's surface and the generated TLE elements therefore are determined relative to the true equator. The direction of the vernal equinox is not tied to the Earth's surface and therefore an approximation (mean equinox) of its direction has to be made.[4]

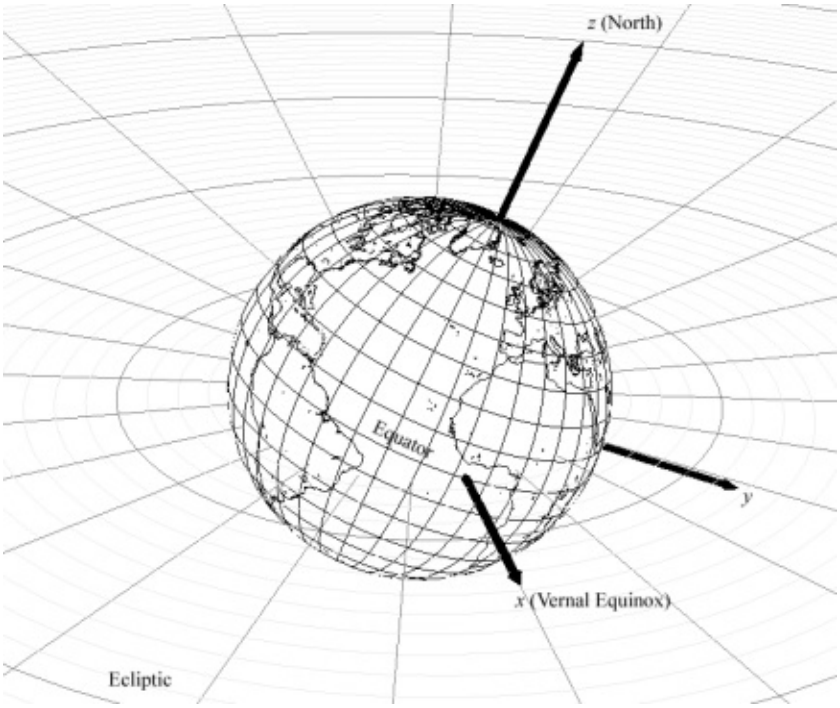

Figure A.1: Earth-Centered Inertial Coordinate System.[4]

[4]https://celestrak.com/columns/v02n01/

A.2. Topocentric Horizon Coordinate System

This system has its origin at a location on the Earth's surface and rotates with the Earth. It is used for satellite observations because it allows to define the looking angles of an antenna pointing in the direction of a satellite in terms of azimuth (β) and elevation (el). The fundamental plane is formed by the local horizon at the observer's location, see Figure A.2. The $\hat{S}$ axis points towards south and the $\hat{Z}$ axis points in the direction of zenith. The $\hat{E}$ axis points east and it is undefined at the North and South Pole. The elevation angle is the angle between the local horizon and the line of sight from the location on Earth to the object of interest. For visible objects the elevation is in a range from 0 to 90 degrees. The (north) azimuth angle is measured from north, increasing eastwards, to the vector from the observer to the object of interest, projected on the local horizon plane.

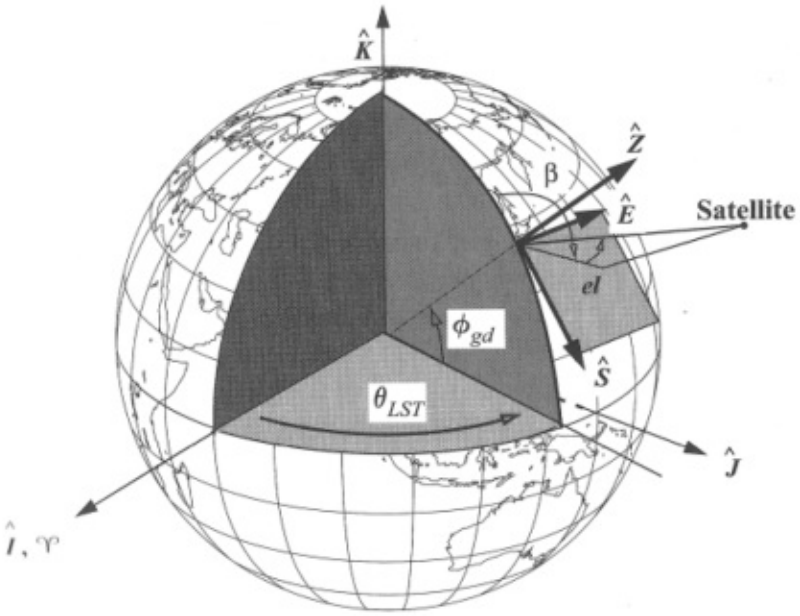

Figure A.2: Topocentric Horizon Coordinate System, SEZ, which moves with Earth and has its origin on the Earth's surface, from Vallado (2013). The local sidereal time θ_{LST} and the geodetic latitude ϕ_{gd} are used to orient the system to a fixed location.

References

Altamimi, Z., & Ray, J. (2004). Evaluation of Colocation Ties Relating the VLBI and GPS Frames. *AGU Fall Meeting Abstracts*.

Altamimi, Z., Rebischung, P., Métivier, L., & Collilieux, X. (2016). ITRF2014: A new release of the International Terrestrial Reference Frame modeling non-linear station motions: ITRF2014. *Journal of Geophysical Research: Solid Earth*, *121*. https://doi.org/10.1002/2016JB013098

Belli, F. (2020). *Transfer of absolute orientation to Galileo orbits with VLBI* (Master thesis). Technical University of Munich.

Biancale, R., Pollet, A., Coulot, D., & Mandea, M. (2017). E-GRASP/Eratosthenes: A mission proposal for millimetric TRF realization. *EGU General Assembly Conference Abstracts*, *19*, 8752.

Böhm, J., Böhm, S., Boisits, J., Girdiuk, A., Gruber, J., Hellerschmied, A., Krasna, H., Landskron, D., Madzak, M., Mayer, D., McCallum, J., McCallum, L., Schartner, M., & Teke, K. (2018). Vienna VLBI and Satellite Software (VieVS) for Geodesy and Astrometry. *Publications of the Astronomical Society of the Pacific*, *130*, 044503. https://doi.org/10.1088/1538-3873/aaa22b

Charlot, P., Jacobs, C. S., Gordon, D., Lambert, S., de Witt, A., Böhm, J., Fey, A. L., Heinkelmann, R., Skurikhina, E., Titov, O., Arias, E. F., Bolotin, S., Bourda, G., Ma, C., Malkin, Z., Nothnagel, A., Mayer, D., MacMillan, D. S., Nilsson, T., & Gaume, R. (2020). The third realization of the International Celestial Reference Frame by very long baseline interferometry. *A&A*, *644*, A159. https://doi.org/10.1051/0004-6361/202038368

Deller, A., Brisken, W. F., Phillips, C. J., Morgan, J., Alef, W., Cappallo, R., Middelberg, E., Romney, J., Rottmann, H., Tingay, S. J., & Wayth, R. (2011). DiFX-2: A More Flexible, Efficient, Robust, and Powerful Software Correlator. *Publications of the Astronomical Society of the Pacific*, *123*(901), 275–287. https://doi.org/10.1086/658907

Deller, A., Tingay, S., & Bailes, M. (2007). DiFX: A Software Correlator for Very Long Baseline Interferometry Using Multiprocessor Computing Environments. *Publications of The Astronomical Society of The Pacific*, *119*, 318–336. https://doi.org/10.1086/513572

Hellerschmied, A. (2014). *Observation of GNSS satellites with VLBI antennas - From observation planning to practical implementation* (Master thesis). Technical University of Vienna.

Hellerschmied, A. (2018). *Satellite Observation with VLBI* (Doctoral thesis). Technical University of Vienna. http://repositum.tuwien.ac.at/urn:nbn:at:at-ubtuw:1-118370

Hellerschmied, A., Böhm, J., Neidhardt, A., Kodet, J., Haas, R., & Plank, L. (2017). Scheduling VLBI Observations to Satellites with VieVS. In T. van Dam (Ed.), *REFAG 2014* (pp. 59–64). Springer International Publishing.

Herring, T. A., Davis, J. L., & Shapiro, I. I. (1990). Geodesy by radio interferometry: The application of Kalman Filtering to the analysis of very long baseline interferometry data. *Journal of Geophysical Research: Solid Earth*, *95*(B8), 12561–12581. https://doi.org/https://doi.org/10.1029/JB095iB08p12561

Hobiger, T., Kondo, T., & Schuh, H. (2006). Very long baseline interferometry as a tool to probe the ionosphere. *Radio Science*, *41*(1). https://doi.org/https://doi.org/10.1029/2005RS003297

Hoots, F. R., & Roehrich, R. L. (1980). *Spacetrack Report No. 3: Models for propagation of NORAD element sets* (tech. rep.). Aerospace Defense Center, Peterson Air Force Base.

Klopotek, G. (2020). *Observations of Artificial Radio Sources within the Framework of Geodetic Very Long Baseline Interferometry* (Doctoral thesis). Chalmers University of Technology.

Krásná, H., Böhm, J., Plank, L., Nilsson, T., & Schuh, H. (2014). Atmospheric Effects on VLBI-Derived Terrestrial and Celestial Reference Frames. In C. Rizos & P. Willis (Eds.), *Earth on the edge: Science for a sustainable planet* (pp. 203–208). Springer Berlin Heidelberg.

Lovell, J., McCallum, J., Reid, P., Mcculloch, P., Baynes, B., Dickey, J., Shabala, S., Watson, C., Titov, O., Ruddick, R., Twilley, R., Reynolds, C., Tingay, S., Shield, P., Adada, R., Ellingsen, S., Morgan, J., & Bignall, H. (2013). The AuScope geodetic VLBI array. *Journal of Geodesy*, *87*. https://doi.org/10.1007/s00190-013-0626-3

Mayer, D. (2019). *VLBI Celestial Reference Frames and Assessment with Gaia* (Doctoral thesis). Technical University of Vienna. https://repositum.tuwien.ac.at/urn:nbn:at:at-ubtuw:1-121147

Nerem, R., Bar-Sever, Y., & Team, G. (2011). The geodetic reference antenna in space (GRASP) - a mission to enhance the terrestrial reference frame. *AGU Fall Meeting Abstracts*.

Niell, A., Whithney, A., Petrachenko, B., Schluter, W., Vandenberg, N., Hase, H., Koyama, Y., Ma, C., Schuh, H., & Tuccari, G. (2005). *VLBI2010: current and future requirements for geodetic VLBI systems. Tech. Rep.*

Nilsson, T., Haas, R., & Elgered, G. (2007). Simulations of atmospheric path delays using turbulence models. *Proceedings of the 18th European VLBI for Geodesy and Astrometry Work Meeting*, 175–180.

Nothnagel, A. (2019). The correlation process in Very Long Baseline Interferometry. *GEM - International Journal on Geomathematics*, *10*. https://doi.org/10.1007/s13137-019-0130-x

Nothnagel, A., Artz, T., Behrend, D., & Malkin, Z. (2017). International VLBI Service for Geodesy and Astrometry: Delivering high-quality products and embarking on observations of the next generation. *Journal of Geodesy*, *91(7)*, 711–721. https://doi.org/10.1007/s00190-016-0950-5

Pany, A., Böhm, J., Macmillan, D., Schuh, H., Nilsson, T., & Wresnik, J. (2010). Monte Carlo simulations of the impact of troposphere, clock and measurement errors on the repeatability of VLBI positions. *Journal of Geodesy*, *85*, 39–50. https://doi.org/10.1007/s00190-010-0415-1

Pearlman, M. R., J., D. J., & Bosworth, J. M. (2002). The International Laser Ranging Service. *Advances in Space Research*, *30*(2), 135–143. https://doi.org/https://doi.org/10.1016/S0273-1177(02)00277-6

Petit, G., & Luzum, B. (2010). IERS conventions (2010). *Tech. Rep. DTIC Document*, *36*, 180.

Petrachenko, B. *Radio antennas, feed horns, and front-end receivers.* In EGU and IVS Training School on VLBI for Geodesy and Astrometry, Aalto University, Finland. 2013.

Plag, H.-P., & Pearlman, M. R. (2009). *Global geodetic observing system: Meeting the requirements of a global society on a changing planet in 2020*. https://doi.org/10.1007/978-3-642-02687-4

Plank, L. (2013). *VLBI satellite tracking for the realization of frame ties* (Doctoral thesis). Technical University of Vienna. http://www.ub.tuwien.ac.at/diss/AC11121594.pdf

Plank, L., Lovell, J., McCallum, J., Mayer, D., Reynolds, C., Quick, J., Weston, S., Titov, O., Shabala, S., Böhm, J., Natusch, T., Nickola, M., & Gulyaev, S. (2017). The AUSTRAL VLBI observing program. *Journal of Geodesy*, *91*, 803–817. https://doi.org/10.1007/s00190-016-0949-y

Ricklefs, R. (2006). Consolidated Laser Ranging Prediction Format Version 1.01. https://ilrs.gsfc.nasa.gov/docs/2006/cpf_1.01.pdf

Salzberg, I. M. (1967). *Mathematical relationships of the MFOD ANTENNA axes* (tech. rep. NASA-TM-X-55956). NASA Goddard Space Flight Center Greenbelt, MD, United States.

Schartner, M. (2019). *Optimizing geodetic VLBI schedules with VieSched++* (Doctoral thesis). Technical University of Vienna. https://repositum.tuwien.at/handle/20.500.12708/1466

Schartner, M., & Böhm, J. (2019). VieSched++: A New VLBI Scheduling Software for Geodesy and Astrometry. *Publications of the Astronomical Society of the Pacific*, *131*, 084501. https://doi.org/10.1088/1538-3873/ab1820

Schuh, H., & Behrend, D. (2012). VLBI: A fascinating technique for geodesy and astrometry. *Journal of Geodynamics*, *61*, 68–80. https://doi.org/10.1016/j.jog.2012.07.007

Schuh, H., & Böhm, J. (2013). Very Long Baseline Interferometry for Geodesy and Astrometry. In G. Xu (Ed.), *Sciences of Geodesy - II: Innovations and Future Developments* (pp. 339–376). Springer Berlin Heidelberg. https://doi.org/10.1007/978-3-642-28000-9_7

Seitz, M., Angermann, D., Bloßfeld, M., Drewes, H., & Gerstl, M. (2012). The 2008 DGFI realization of the ITRS: DTRF2008. *Journal of Geodesy*, *138*, 87–93. https://doi.org/10.1007/s00190-012-0567-2

Spicakova, H., Böhm, J., Böhm, S., Nilsson, T., Pany, A., Plank, L., Teke, K., & Schuh, H. (2010). Estimation of Geodetic and Geodynamical Parameters with VieVS. *2010 General Meeting Proceedings, Hobart, Tasmania, Australia, February 7-13, 2010*, 202–206.

Spofford, P., & Remondi, B. (1995). The National Geodetic Survey Standard GPS Format SP3. NOAA, National Geodetic Survey. ftp://igscb.jpl.nasa.gov/igscb/data/format/sp3_docu.txt

Sun, J. (2013). *VLBI scheduling strategies with respect to VLBI2010* (Doctoral thesis). Technical University of Vienna. http://www.ub.tuwien.ac.at/diss/AC07814953.pdf

Vallado, D. (2013). *Fundamentals of Astrodynamics and Applications*. Microcosm Press, 4th Ed.

Vandenberg, N. (1999). sked: Interactive/Automatic Scheduling Program. NVI, Inc. NASA/Goddard Space Flight Center.

Walker, R. (2018). *The SCHED user manual* (tech. rep.).